

Primordial Gravitational Waves and Rescattered Electromagnetic Radiation in the Cosmic Microwave Background

Dong-Hoon Kim¹ and Sascha Trippe^{2,3}

¹*Basic Science Research Institute,
Ewha Womans University, Seoul 03760,
Republic of Korea; ki13130@gmail.com*

²*Department of Physics and Astronomy,
Seoul National University, Seoul 08826,
Republic of Korea; trippe@astro.snu.ac.kr*

³*Corresponding author*

Understanding the interaction of primordial gravitational waves (GWs) with the Cosmic Microwave Background (CMB) plasma is important for observational cosmology. In this article, we provide an analysis of an effect apparently overlooked as yet. We consider a single free electric charge and suppose that it can be agitated by primordial GWs propagating through the CMB plasma, resulting in periodic, regular motion along particular directions. Light reflected by the charge will be partially polarized, and this will imprint a characteristic pattern on the CMB. We study this effect by considering a simple model in which anisotropic incident electromagnetic (EM) radiation is rescattered by a charge sitting in spacetime perturbed by GWs and becomes polarized. As the charge is driven to move along particular directions, we calculate its dipole moment to determine the leading-order rescattered EM radiation. The Stokes parameters of the rescattered radiation exhibit a net linear polarization. We investigate how this polarization effect can be schematically represented out of the Stokes parameters. We work out the representations of gradient modes (E-modes) and curl modes (B-modes) to produce polarization maps. Although the polarization effect results from GWs, we find that its representations, the E- and B-modes, do not practically reflect the GW properties such as strain amplitude, frequency and polarization states.

I. INTRODUCTION

Ever since its experimental detection [25] and subsequent interpretation as a relic of the earliest epoch of the universe [10], studies of the Cosmic Microwave Background (CMB) have been crucial for constraining cosmological models. Present-day space-based measurements of the angular power spectrum of the CMB temperature distribution on the sky are able to constrain the parameters included in the Λ CDM model of cosmology [5] with statistical uncertainties down to a few per cent [1]. Of special importance is the fact that state-of-the-art cosmological observations can, at least in principle, place constraints on the large family of models of cosmic inflation [20] which is a cornerstone of hot big-bang cosmology.

A key prediction made by models of inflation is the occurrence of primordial gravitational waves (GWs). Even though not observable directly (currently), they should be detectable indirectly via a characteristic linear polarization of the CMB [26]. CMB polarization can be decomposed into contributions from gradient modes (E-modes) and curl modes (B-modes), with the latter ones being excited by either tensor perturbations, i.e., propagation of primordial GWs through the plasma emitting the CMB, or gravitational lensing by foreground matter [17, 29]. Polarimetric observations [28] of the CMB at radio frequencies around 100 GHz have been numerous, with different classes of observations aimed at different polarization modes (E or B) and angular scales. A first observation of E-mode polarization was achieved by the Degree Angular Scale Interferometer in 2002 [19]. B-mode polarization due to gravitational lensing was first detected by the South Pole Telescope in 2013 [14] and has since been observed by POLARBEAR [3, 4], ACTPol [21], and BICEP1 [6]. A detection of B-mode polarization caused by primordial GWs was claimed by the BICEP2 collaboration in 2014 [2] but was shown to be likely caused by interstellar dust soon thereafter [11].

The aforementioned studies aim at comparisons of theoretical polarization – specifically B-mode – patterns to observational ones in order to constrain cosmological quantities. In a nutshell, the polarization patterns studied so far

originate as follows: GWs propagating through the CMB plasma cause local quadrupole anisotropies in the radiation field; this in turn causes characteristic polarization patterns in the light scattered at CMB plasma electrons. However, at least a priori one should also expect polarization immediately from interactions between GWs and individual electric charges. An electric charge located in the path of propagation of a GW will be forced into an oscillatory motion by the wave. This should lead to characteristic linear polarization of light scattered by the charge. We herewith present what appears to be the first quantitative analysis of this effect. We work out the representations of gradient modes (E-modes) and curl modes (B-modes) to produce maps of the polarization patterns resulting from scattering at a single electric charge. Throughout this work, we adopt the negative metric signature $(-, +, +, +)$, and the Minkowski metric is given by $\eta_{\mu\nu} = \text{diag}(-1, 1, 1, 1)$.

II. RESCATTERED EM RADIATION AND POLARIZATION IN THE CMB

A. EM radiation rescattered by a charge in perturbed spacetime

Consider an electric charge q with mass m in the CMB plasma. If the charge encounters incident light, it reradiates (outgoing) reflected light. If, however, the charge is set in oscillating motion by a GW, the geometry of reflection will be given by the GW: as the charge is driven to move along particular directions, like the GW polarizations h_+ or h_\times , it will reradiate the reflected light along the same directions.

The electromagnetic (EM) radiation rescattered by the charge, as measured by a distant observer, can be obtained by solving the Maxwell equations

$$\square A_\mu = -\frac{4\pi}{c} j_\mu, \quad (1)$$

where $\square \equiv -\partial^2/c^2 \partial t^2 + \partial^2/\partial x^2 + \partial^2/\partial y^2 + \partial^2/\partial z^2$ denotes the d'Alembertian, with c representing the speed of light, and A_μ represents the EM vector potential produced by the charge and j_μ the charge's current density. A solution to the Maxwell's equations can be expressed to the leading-order as

$$A_\mu \sim \frac{\dot{Q}_\mu(t_R)}{r}, \quad (2)$$

where r is the distance from the charge to the observer and $t_R \equiv t - r/c$ denotes the retarded time, and Q_μ is the charge-dipole moment defined as

$$Q_\mu = qX_\mu \quad (3)$$

for the charge q at position X_μ , and the overdot denotes differentiation with respect to time t .

Our rescattered EM radiation can be computed using Eqs. (2) and (3), with the charge's trajectory $X_\mu(t)$ determined in the spacetime

$$g_{\mu\nu} = \eta_{\mu\nu} + h_{\mu\nu}, \quad (4)$$

where $\eta_{\mu\nu}$ is the flat background and $h_{\mu\nu}$ describes the perturbations by GWs.¹ As the charge is moving in curved spacetime, to treat the general relativistic effects of the charge's motion we employ a semi-relativistic approximation [27], in which the charge's trajectory $X_\mu(t)$ is identified with a geodesic in the spacetime $g_{\mu\nu}$. For a weakly perturbed spacetime, in which $|h_{\mu\nu}| \ll 1$, one may split the dipole moment,

$$Q^\mu = qX_{(\text{flat})}^\mu + q\mathcal{X}^\mu, \quad (5)$$

¹ In this work, to simplify our analysis, the spacetime is given by the metric $ds^2 = (\eta_{\mu\nu} + h_{\mu\nu}) dx^\mu dx^\nu$ rather than $ds^2 = a^2(\tau) [-d\tau^2 + (\delta_{ij} + h_{ij}) dx^i dx^j]$, the Friedmann-Robertson-Walker metric for the expanding universe, where $a(\tau)$ denotes the scale factor, with τ being the conformal time. Here we assume that during the epoch of reionization the universe was expanding at a rate substantially slower than the characteristic frequency of the CMB radiation, $\sim 10^{11}$ Hz. Therefore, to a good approximation, our EM radiation from a 'single' charge can be well-described in the perturbed flat spacetime.

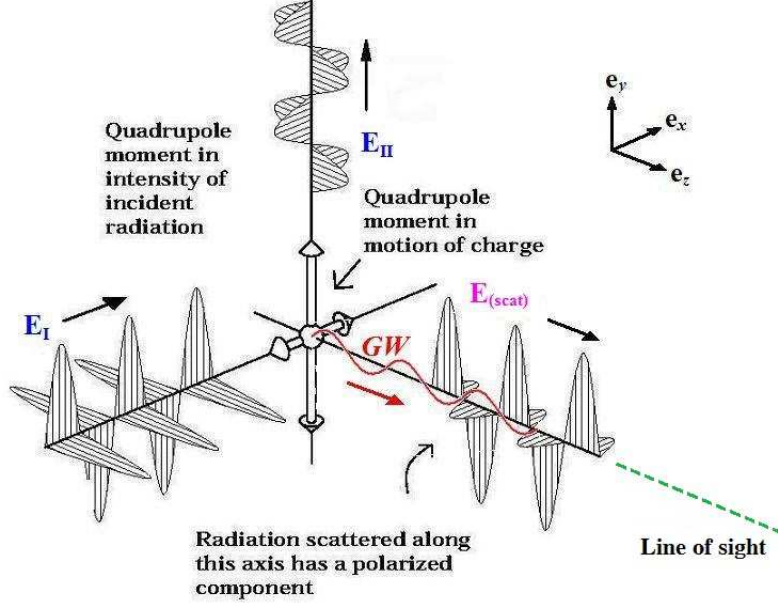


FIG. 1: An anisotropic incident EM radiation is rescattered by a charge sitting on spacetime ripples (i.e. GWs) and becomes polarized. The GWs propagate along the line of sight while being polarized in a plane perpendicular to the line of sight, and the rescattered (outgoing) EM radiation is induced by the GWs. Note that the directions of propagation and polarization of the GWs are fitted into the observer's reference frame; with propagation along the z -axis (coinciding with the line of sight) and polarization along the x -axis and the y -axis. (Credit: CAPMAP website, <http://quiet.uchicago.edu/capmap>; reproduced with some modifications)

and the vector potential accordingly,

$$A^\mu = A_{(\text{flat})}^\mu + \mathcal{A}^\mu, \quad (6)$$

where the perturbation \mathcal{A}^μ to the potential $A_{(\text{flat})}^\mu$ results from the deviation \mathcal{X}^μ from the trajectory $X_{(\text{flat})}^\mu$ which is caused by the perturbation of the flat background $\eta_{\mu\nu}$ by GWs $h_{\mu\nu}$.

Now, we prescribe an anisotropic incident monochromatic radiation field on a charge as shown in Figure 1 by means of the two waves,

$$\mathbf{E}_{I(\text{in})} = E_I \{ \mathbf{e}_y \exp [i(Kx - \Omega t + \varphi_I(t)) + \mathbf{e}_z \exp [i(Kx - \Omega t + \vartheta_I(t))]\}, \quad (7)$$

$$\mathbf{E}_{II(\text{in})} = E_{II} \{ \mathbf{e}_x \exp [i(Ky - \Omega t + \varphi_{II}(t))] + \mathbf{e}_z \exp [i(Ky - \Omega t + \vartheta_{II}(t))]\}, \quad (8)$$

where E_I and E_{II} ($E_I \neq E_{II}$) are the amplitudes, and Ω and K are the angular temporal frequency and angular spatial frequency with $\Omega = cK$, and $\varphi_I(t)$, $\vartheta_I(t)$, $\varphi_{II}(t)$ and $\vartheta_{II}(t)$ are the phase modulation functions, which are assumed to vary on a time scale much slower than the period of the waves, i.e. $|\dot{\varphi}_I|$, $|\dot{\vartheta}_I|$, $|\dot{\varphi}_{II}|$, $|\dot{\vartheta}_{II}| \ll \Omega$. Here each of $\mathbf{E}_{I(\text{in})}$ and $\mathbf{E}_{II(\text{in})}$ is *unpolarized*: as the relative phases $\varphi_I(t) - \vartheta_I(t)$ and $\varphi_{II}(t) - \vartheta_{II}(t)$ fluctuate in time, each wave will not remain in a single polarization state and hence is unpolarized. That is, the Stokes parameters for each wave must exhibit

$$\begin{bmatrix} I_{(\text{in})} \\ Q_{(\text{in})} \\ U_{(\text{in})} \\ V_{(\text{in})} \end{bmatrix} \sim \begin{bmatrix} 1 \\ 0 \\ 0 \\ 0 \end{bmatrix}, \quad (9)$$

which can be verified via Eqs. (40) - (43) (see Appendix A).

1. *Case 1. For GWs propagating along the line of sight*

As mentioned above, to calculate the EM radiation rescattered by a charge moving in curved spacetime, we determine the charge's trajectory $X_\mu(t)$, which is indeed identified with a geodesic worldline that the charge follows in the spacetime $g_{\mu\nu} = \eta_{\mu\nu} + h_{\mu\nu}$, where $h_{\mu\nu}$ represents GWs [27]. For a weakly perturbed spacetime, in which $|h_{\mu\nu}| \ll 1$, one can write down the geodesic equation of motion for the charge in linearized gravity as follows [24]:

$$\ddot{X}^i + \eta^{ik} h_{jk,t} \dot{X}^j + \frac{1}{2} \eta^{il} (h_{jl,k} + h_{kl,j} - h_{jk,l}) \dot{X}^j \dot{X}^k = \frac{q}{m} (\eta^{ik} - h^{ik}) E_k, \quad (10)$$

where the indices i, j, \dots refer to the spatial coordinates (x, y, z) , and the overdot $\dot{\cdot}$ represents differentiation with respect to time t , and the comma before subscripts indicates partial differentiation with respect to the subscript that follows the comma. In this equation the GWs h_{ij} are given by

$$h_{ij}^+ = h (e_i^1 \otimes e_j^1 - e_i^2 \otimes e_j^2) \exp \left[i\omega \left(\frac{z}{c} - t \right) \right], \quad (11)$$

$$h_{ij}^\times = h (e_i^1 \otimes e_j^2 + e_i^2 \otimes e_j^1) \exp \left[i\omega \left(\frac{z}{c} - t \right) \right], \quad (12)$$

where h denotes the strain amplitude, ω the frequency,² $e_i^{1(2)}$ refers to the $x(y)$ -component of the unit vector \mathbf{e}_i , and $+$ and \times represent the two polarization states prescribed by the tensors $e_i^1 \otimes e_j^1 - e_i^2 \otimes e_j^2$ and $e_i^1 \otimes e_j^2 + e_i^2 \otimes e_j^1$, respectively. On the right-hand side of Eq. (10) the EM field is prescribed by means of Eqs. (7) and (8)) as

$$E_i = e_i^2 E_I \exp \left[i \left(\Omega \left(\frac{z}{c} - t \right) + \varphi_I(t) \right) \right] + e_i^1 E_{II} \exp \left[i \left(\Omega \left(\frac{z}{c} - t \right) + \varphi_{II}(t) \right) \right], \quad (13)$$

which describes the outgoing field reflected by the charge: the charge is driven to move along the x -axis and the y -axis by GWs h_+ or h_\times , and hence reradiates the outgoing reflected light most easily by moving along the same directions. The incident and outgoing EM radiation fields and the GWs are illustrated in Figure 1: the GWs propagate along the line of sight while being polarized in a plane perpendicular to the line of sight, and the rescattered (outgoing) EM radiation is induced by the GWs. Note here that the directions of propagation and polarization of the GWs are fitted into the observer's reference frame; with propagation along the z -axis (coinciding with the line of sight) and polarization along the x -axis and the y -axis.

Now, solving the geodesic equation (10) via perturbation, we obtain the following results (see Appendix B for a detailed derivation):

² In this work, for the sake of simplification, the strain amplitude h is assumed to be a constant over a finite number of periods $\sim 2n\pi/\omega$. Practically, it may be equivalently stated that h changes little for $\sim 10^{13}$ seconds: taking into account the redshift effect from cosmic expansion, the frequency ω should be $\sim 10^3$ times higher than the characteristic frequency for the regime of the CMB anisotropies in the spectrum as shown in Figure 3. Later in this Section, the Stokes parameters are computed for the rescattered EM radiation. They are time-averaged quantities evaluated over a duration on the same time scale, which is substantially longer than the characteristic period of the CMB radiation $\sim 10^{-11}$ seconds.

For h_+ ,

$$\begin{aligned} \dot{x} = & v_{ox} - hv_{ox} \left(1 - \frac{v_{oz}}{c}\right) \exp \left[i\omega \left(\frac{z}{c} - t\right) \right] + i \frac{qE_{II}}{m\Omega} \left\{ \exp \left[i \left(\Omega \left(\frac{z}{c} - t\right) + \varphi_{II}(t) \right) \right] \right. \\ & \left. - h \left(1 - \frac{v_{oz}\omega}{c(\Omega + \omega)}\right) \exp \left[i \left((\Omega + \omega) \left(\frac{z}{c} - t\right) + \varphi_{II}(t) \right) \right] \right\} + \mathcal{O}_{II[0]} + \mathcal{O}_{II[h]}, \end{aligned} \quad (14)$$

$$\begin{aligned} \dot{y} = & v_{oy} + hv_{oy} \left(1 - \frac{v_{oz}}{c}\right) \exp \left[i\omega \left(\frac{z}{c} - t\right) \right] + i \frac{qE_I}{m\Omega} \left\{ \exp \left[i \left(\Omega \left(\frac{z}{c} - t\right) + \varphi_I(t) \right) \right] \right. \\ & \left. + h \left(1 - \frac{v_{oz}\omega}{c(\Omega + \omega)}\right) \exp \left[i \left((\Omega + \omega) \left(\frac{z}{c} - t\right) + \varphi_I(t) \right) \right] \right\} + \mathcal{O}_{I[0]} + \mathcal{O}_{I[h]}, \end{aligned} \quad (15)$$

$$\begin{aligned} \dot{z} = & v_{oz} - \frac{h(v_{ox}^2 - v_{oy}^2)}{2c} \exp \left[i\omega \left(\frac{z}{c} - t\right) \right] \\ & - i \frac{hq\omega}{mc\Omega(\Omega + \omega)} \left\{ E_{II}v_{ox} \exp \left[i \left((\Omega + \omega) \left(\frac{z}{c} - t\right) + \varphi_{II}(t) \right) \right] \right. \\ & \left. - E_Iv_{oy} \exp \left[i \left((\Omega + \omega) \left(\frac{z}{c} - t\right) + \varphi_I(t) \right) \right] \right\} \\ & + \frac{hq^2\omega}{2m^2c\Omega^2(2\Omega + \omega)} \left\{ E_{II}^2 \exp \left[i \left((2\Omega + \omega) \left(\frac{z}{c} - t\right) + 2\varphi_{II}(t) \right) \right] \right. \\ & \left. - E_I^2 \exp \left[i \left((2\Omega + \omega) \left(\frac{z}{c} - t\right) + 2\varphi_I(t) \right) \right] \right\} + \mathcal{O}_{I,II[0]} + \mathcal{O}_{I,II[h]}, \end{aligned} \quad (16)$$

For h_\times ,

$$\begin{aligned} \dot{x} = & v_{ox} - hv_{oy} \left(1 - \frac{v_{oz}}{c}\right) \exp \left[i\omega \left(\frac{z}{c} - t\right) \right] + i \frac{qE_{II}}{m\Omega} \left\{ \exp \left[i \left(\Omega \left(\frac{z}{c} - t\right) + \varphi_{II}(t) \right) \right] \right. \\ & \left. - h \frac{E_I}{E_{II}} \left(1 - \frac{v_{oz}\omega}{c(\Omega + \omega)}\right) \exp \left[i \left((\Omega + \omega) \left(\frac{z}{c} - t\right) + \varphi_I(t) \right) \right] \right\} + \mathcal{O}_{I,II[0]} + \mathcal{O}_{I,II[h]}, \end{aligned} \quad (17)$$

$$\begin{aligned} \dot{y} = & v_{oy} - hv_{ox} \left(1 - \frac{v_{oz}}{c}\right) \exp \left[i\omega \left(\frac{z}{c} - t\right) \right] + i \frac{qE_I}{m\Omega} \left\{ \exp \left[i \left(\Omega \left(\frac{z}{c} - t\right) + \varphi_I(t) \right) \right] \right. \\ & \left. - h \frac{E_{II}}{E_I} \left(1 - \frac{v_{oz}\omega}{c(\Omega + \omega)}\right) \exp \left[i \left((\Omega + \omega) \left(\frac{z}{c} - t\right) + \varphi_{II}(t) \right) \right] \right\} + \mathcal{O}_{I,II[0]} + \mathcal{O}_{I,II[h]}, \end{aligned} \quad (18)$$

$$\begin{aligned} \dot{z} = & v_{oz} - \frac{hv_{ox}v_{oy}}{c} \exp \left[i\omega \left(\frac{z}{c} - t\right) \right] \\ & - i \frac{hq\omega}{mc\Omega(\Omega + \omega)} \left\{ E_Iv_{ox} \exp \left[i \left((\Omega + \omega) \left(\frac{z}{c} - t\right) + \varphi_I(t) \right) \right] \right. \\ & \left. + E_{II}v_{oy} \exp \left[i \left((\Omega + \omega) \left(\frac{z}{c} - t\right) + \varphi_{II}(t) \right) \right] \right\} \\ & + \frac{hq^2E_I E_{II}\omega}{m^2c\Omega^2(2\Omega + \omega)} \exp \left[i \left((2\Omega + \omega) \left(\frac{z}{c} - t\right) + \varphi_I(t) + \varphi_{II}(t) \right) \right] + \mathcal{O}_{I,II[0]} + \mathcal{O}_{I,II[h]}, \end{aligned} \quad (19)$$

where (v_{ox}, v_{oy}, v_{oz}) represents the charge's constant drifting velocity, and $\mathcal{O}_{I[0]} \equiv \mathcal{O}(\dot{\varphi}_I/\Omega, \ddot{\varphi}_I/\Omega^2, \dot{\varphi}_I\ddot{\varphi}_I/\Omega^3, \ddot{\varphi}_I/\Omega^3, \dots)$, $\mathcal{O}_{II[0]} \equiv \mathcal{O}(\dot{\varphi}_{II}/\Omega, \ddot{\varphi}_{II}/\Omega^2, \dot{\varphi}_{II}\ddot{\varphi}_{II}/\Omega^3, \ddot{\varphi}_{II}/\Omega^3, \dots)$, $\mathcal{O}_{I,II[0]} \equiv \mathcal{O}(\dot{\varphi}_I/\Omega, \ddot{\varphi}_I/\Omega^2, \dot{\varphi}_I\ddot{\varphi}_I/\Omega^3, \ddot{\varphi}_I/\Omega^3, \dots, \dot{\varphi}_{II}/\Omega, \ddot{\varphi}_{II}/\Omega^2, \dot{\varphi}_{II}\ddot{\varphi}_{II}/\Omega^3, \ddot{\varphi}_{II}/\Omega^3, \dots)$, $\mathcal{O}_{I[h]} \sim h \times \mathcal{O}_{I[0]}$, $\mathcal{O}_{II[h]} \sim h \times \mathcal{O}_{II[0]}$, $\mathcal{O}_{I,II[h]} \sim h \times \mathcal{O}_{I,II[0]}$ are the errors generated by the approximate solution for $\dot{X}^i = (\dot{x}, \dot{y}, \dot{z})$: the subscripts $_{[0]}$ and $_{[h]}$ denote that the errors are generated from the unperturbed part and the perturbed part of the solution, respectively. Above, however, we have assumed that the phase modulation functions $\varphi_I(t)$ and $\varphi_{II}(t)$ vary on a time scale much slower than the period of the wave, namely, $|\dot{\varphi}_I|, |\dot{\varphi}_{II}| \ll \Omega$ (and further $|\ddot{\varphi}_I|, |\ddot{\varphi}_{II}| \ll \Omega^2$, $|\ddot{\varphi}_I|, |\ddot{\varphi}_{II}| \ll \Omega^3$, etc.), and therefore all these errors can be regarded as sufficiently small. A more detailed discussion of the errors is given in Appendix B.

The rescattered EM potentials are calculated by substituting Eqs. (14) – (19) into Eq. (2). They are trivially

obtained from

$$A_x(\text{scat}) = \frac{q\dot{x}(t_R)}{r}, \quad (20)$$

$$A_y(\text{scat}) = \frac{q\dot{y}(t_R)}{r}, \quad (21)$$

$$A_z(\text{scat}) = \frac{q\dot{z}(t_R)}{r}, \quad (22)$$

together with Eqs. (14), (15), (16) for h_+ and Eqs. (17), (18), (19) for h_\times .

Finally, the rescattered EM fields are calculated by means of $F_{ab} = \nabla_a A_b - \nabla_b A_a$ and Eqs. (20), (21), (22). They are obtained from

$$E_x(\text{scat}) = \partial_t A_x(\text{scat}) = \frac{q\ddot{x}(t_R)}{r}, \quad (23)$$

$$E_y(\text{scat}) = \partial_t A_y(\text{scat}) = \frac{q\ddot{y}(t_R)}{r}, \quad (24)$$

$$E_z(\text{scat}) = \partial_t A_z(\text{scat}) = \frac{q\ddot{z}(t_R)}{r}, \quad (25)$$

together with Eqs. (14), (15), (16) for h_+ and Eqs. (17), (18), (19) for h_\times . The results are the following (see Appendix B for a detailed derivation):

For h_+ ,

$$\begin{aligned} E_x(\text{scat}) = & i \frac{hqv_{ox} \left(1 - \frac{v_{oz}}{c}\right) \omega}{r} \exp \left[i\omega \left(\frac{z}{c} - t_R \right) \right] + \frac{q^2 E_{II}}{mr} \left\{ \exp \left[i \left(\Omega \left(\frac{z}{c} - t_R \right) + \varphi_{II}(t_R) \right) \right] \right. \\ & \left. - h \left(1 + \left(1 - \frac{v_{oz}}{c} \right) \frac{\omega}{\Omega} \right) \exp \left[i \left((\Omega + \omega) \left(\frac{z}{c} - t_R \right) + \varphi_{II}(t_R) \right) \right] \right\} + \mathcal{O}_{II[h]}, \end{aligned} \quad (26)$$

$$\begin{aligned} E_y(\text{scat}) = & -i \frac{hqv_{oy} \left(1 - \frac{v_{oz}}{c}\right) \omega}{r} \exp \left[i\omega \left(\frac{z}{c} - t_R \right) \right] + \frac{q^2 E_I}{mr} \left\{ \exp \left[i \left(\Omega \left(\frac{z}{c} - t_R \right) + \varphi_I(t_R) \right) \right] \right. \\ & \left. + h \left(1 + \left(1 - \frac{v_{oz}}{c} \right) \frac{\omega}{\Omega} \right) \exp \left[i \left((\Omega + \omega) \left(\frac{z}{c} - t_R \right) + \varphi_I(t_R) \right) \right] \right\} + \mathcal{O}_{I[h]}, \end{aligned} \quad (27)$$

$$\begin{aligned} E_z(\text{scat}) = & i \frac{hq(v_{ox}^2 - v_{oy}^2) \omega}{2cr} \exp \left[i\omega \left(\frac{z}{c} - t_R \right) \right] \\ & - \frac{hq^2 \omega}{mcr\Omega} \left\{ E_{II} v_{ox} \exp \left[i \left((\Omega + \omega) \left(\frac{z}{c} - t_R \right) + \varphi_{II}(t_R) \right) \right] \right. \\ & \left. - E_I v_{oy} \exp \left[i \left((\Omega + \omega) \left(\frac{z}{c} - t_R \right) + \varphi_I(t_R) \right) \right] \right\} \\ & - i \frac{hq^3 \omega}{2m^2 cr \Omega^2} \left\{ E_{II}^2 \exp \left[i \left((2\Omega + \omega) \left(\frac{z}{c} - t_R \right) + 2\varphi_{II}(t_R) \right) \right] \right. \\ & \left. - E_I^2 \exp \left[i \left((2\Omega + \omega) \left(\frac{z}{c} - t_R \right) + 2\varphi_I(t_R) \right) \right] \right\} + \mathcal{O}_{I,II[h]}, \end{aligned} \quad (28)$$

For h_\times ,

$$E_{x(\text{scat})} = i \frac{hqv_{oy} \left(1 - \frac{v_{oz}}{c}\right) \omega}{r} \exp \left[i\omega \left(\frac{z}{c} - t_R \right) \right] + \frac{q^2 E_{\text{II}}}{mr} \left\{ \exp \left[i \left(\Omega \left(\frac{z}{c} - t_R \right) + \varphi_{\text{II}}(t_R) \right) \right] \right. \\ \left. - h \frac{E_{\text{I}}}{E_{\text{II}}} \left(1 + \left(1 - \frac{v_{oz}}{c} \right) \frac{\omega}{\Omega} \right) \exp \left[i \left((\Omega + \omega) \left(\frac{z}{c} - t_R \right) + \varphi_{\text{I}}(t_R) \right) \right] \right\} + \mathcal{O}_{\text{I,II}[h]}, \quad (29)$$

$$E_{y(\text{scat})} = i \frac{hqv_{ox} \left(1 - \frac{v_{oz}}{c}\right) \omega}{r} \exp \left[i\omega \left(\frac{z}{c} - t_R \right) \right] + \frac{q^2 E_{\text{I}}}{mr} \left\{ \exp \left[i \left(\Omega \left(\frac{z}{c} - t_R \right) + \varphi_{\text{I}}(t_R) \right) \right] \right. \\ \left. - h \frac{E_{\text{II}}}{E_{\text{I}}} \left(1 + \left(1 - \frac{v_{oz}}{c} \right) \frac{\omega}{\Omega} \right) \exp \left[i \left((\Omega + \omega) \left(\frac{z}{c} - t_R \right) + \varphi_{\text{II}}(t_R) \right) \right] \right\} + \mathcal{O}_{\text{I,II}[h]}, \quad (30)$$

$$E_{z(\text{scat})} = i \frac{hqv_{ox} v_{oy} \omega}{cr} \exp \left[i\omega \left(\frac{z}{c} - t_R \right) \right] \\ - \frac{hq^2 \omega}{mcr\Omega} \left\{ E_{\text{I}} v_{ox} \exp \left[i \left((\Omega + \omega) \left(\frac{z}{c} - t_R \right) + \varphi_{\text{I}}(t_R) \right) \right] \right. \\ \left. + E_{\text{II}} v_{oy} \exp \left[i \left((\Omega + \omega) \left(\frac{z}{c} - t_R \right) + \varphi_{\text{II}}(t_R) \right) \right] \right\} \\ - i \frac{hq^3 E_{\text{I}} E_{\text{II}} \omega}{m^2 cr \Omega^2} \exp \left[i \left((2\Omega + \omega) \left(\frac{z}{c} - t_R \right) + \varphi_{\text{I}}(t_R) + \varphi_{\text{II}}(t_R) \right) \right] + \mathcal{O}_{\text{I,II}[h]}. \quad (31)$$

Here we note that the errors from the unperturbed part, $\mathcal{O}_{\text{I}[0]}$, $\mathcal{O}_{\text{II}[0]}$ and $\mathcal{O}_{\text{I,II}[0]}$ are absent and only the errors from the perturbed part, $\mathcal{O}_{\text{I}[h]}$, $\mathcal{O}_{\text{II}[h]}$ and $\mathcal{O}_{\text{I,II}[h]}$ are present. This is because $E_{(\text{scat})}^i \sim \ddot{X}^i$ due to Eqs. (23), (24) and (25), where the unperturbed part of a solution for $\ddot{X}^i = (\ddot{x}, \ddot{y}, \ddot{z})$ is trivially obtained from the right-hand side of the geodesic equation (10), which is equivalent to Eq. (13) apart from the factor; thereby not generating $\mathcal{O}_{[0]}$. Later in Subsection II B, we will disregard any contributions from the errors $\mathcal{O}_{\text{I}[h]}$, $\mathcal{O}_{\text{II}[h]}$ and $\mathcal{O}_{\text{I,II}[h]}$ in computing Stokes parameters. A more detailed discussion of the errors is given in Appendix B.

2. Case 2. For GWs propagating along an arbitrary direction

Our physical quantities for *Case 1* above were expressed in the observer's reference frame associated with Cartesian coordinates (x, y, z) : the rescattered EM radiation was induced by GWs which propagate along the z -axis with polarization along the x -axis and the y -axis. This does *not* imply that radiation can only be observed along the z -axis: we now discuss the case that line of sight and z -axis do not coincide. A new reference frame can be defined by rotating the Cartesian frame through Euler angles $\{\phi, \theta, \psi\}$ following the convention by [12]:

$$\mathbf{x}' = \mathbf{R}(\phi, \theta, \psi) \mathbf{x}, \quad (32)$$

where $\mathbf{x}' \equiv (x', y', z')$ refer to the new frame while $\mathbf{x} \equiv (x, y, z)$ the original frame, and

$$\mathbf{R}(\phi, \theta, \psi) = \mathbf{R}_3(\psi) \mathbf{R}_2(\theta) \mathbf{R}_1(\phi) \\ = \begin{bmatrix} \cos \psi \cos \phi - \cos \theta \sin \phi \sin \psi & \cos \psi \sin \phi + \cos \theta \cos \phi \sin \psi & \sin \psi \sin \theta \\ -\sin \psi \cos \phi - \cos \theta \sin \phi \cos \psi & -\sin \psi \sin \phi + \cos \theta \cos \phi \cos \psi & \cos \psi \sin \theta \\ \sin \theta \sin \phi & -\sin \theta \cos \phi & \cos \theta \end{bmatrix}, \quad (33)$$

with

$$\mathbf{R}_1(\phi) \equiv \begin{bmatrix} \cos \phi & \sin \phi & 0 \\ -\sin \phi & \cos \phi & 0 \\ 0 & 0 & 1 \end{bmatrix}, \mathbf{R}_2(\theta) \equiv \begin{bmatrix} 1 & 0 & 0 \\ 0 & \cos \theta & \sin \theta \\ 0 & -\sin \theta & \cos \theta \end{bmatrix}, \mathbf{R}_3(\psi) \equiv \begin{bmatrix} \cos \psi & \sin \psi & 0 \\ -\sin \psi & \cos \psi & 0 \\ 0 & 0 & 1 \end{bmatrix}, \quad (34)$$

and $\{\phi, \theta\}$ denote the direction angles in spherical coordinates, defined with respect to the Cartesian coordinates (x, y, z) , and ψ denotes the polarization-ellipse angle [23].

Let us now consider a more general situation in which GWs propagate along a general direction through the CMB. One may let the propagation direction of our GWs coincide with the z' -axis in the new frame (x', y', z') which is

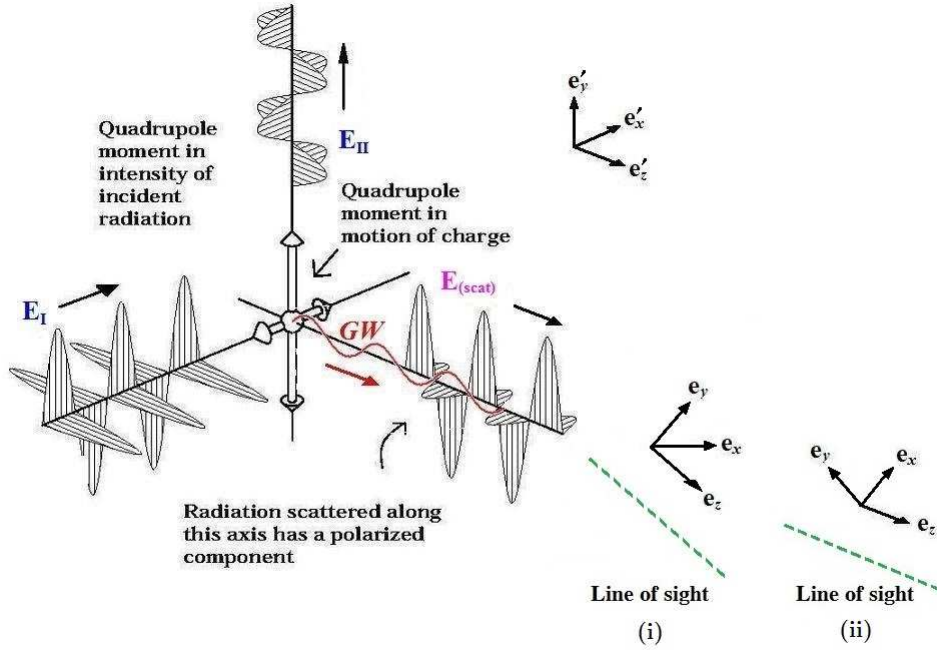


FIG. 2: An anisotropic incident EM radiation is rescattered by a charge sitting on spacetime ripples (i.e. GWs) and becomes polarized. Here the incident and outgoing EM radiation fields and the GWs are illustrated with respect to the source frame (x', y', z') : the GWs propagate along the z' -axis while being polarized along the x' -axis and the y' -axis, and the rescattered (outgoing) EM radiation induced by the GWs should be expressed in the same frame. Concerning the relationship between the source frame (x', y', z') and the observer's frame (x, y, z) , we note the two cases: (i) the propagation direction of the GWs does not coincide with the line of sight, i.e. $\mathbf{e}'_z \neq \mathbf{e}_z$, (ii) the propagation direction of the GWs coincides with the line of sight, i.e. $\mathbf{e}'_z = \mathbf{e}_z$. (Credit: CAPMAP website, <http://quiet.uchicago.edu/capmap>; reproduced with some modifications)

obtained by rotating the original frame (x, y, z) via Eq. (32) above. Then a charge q in the CMB would be driven to move along the x' -axis and the y' -axis by GWs h_+ or h_\times prescribed in the new frame. Therefore, the geodesic equation (10), together with Eqs. (11), (12) and (13) should be rewritten in the coordinates (t, x', y', z') . Solving the geodesic equation in the new frame, one should obtain the same results as (14) - (19) in *Case 1* above, except that the solutions are now expressed in (t, x', y', z') rather than (t, x, y, z) . The same argument goes for the rescattered EM fields (26) - (31). In Figure 2 are illustrated the incident and outgoing EM radiation fields and the GWs with respect to the new coordinate frame, namely the source frame (x', y', z') : the GWs propagate along the z' -axis while being polarized along the x' -axis and the y' -axis, and the rescattered (outgoing) EM radiation induced by the GWs should be expressed in the same frame. Here, concerning the relationship between the source frame (x', y', z') and the observer's frame (x, y, z) , we note the two cases: (i) the propagation direction of the GWs does not coincide with the line of sight, i.e. $\mathbf{e}'_z \neq \mathbf{e}_z$, (ii) the propagation direction of the GWs coincides with the line of sight, i.e. $\mathbf{e}'_z = \mathbf{e}_z$.

Now, the inverse transformation to Eq. (32),

$$\mathbf{x} = \mathbf{R}^{-1}(\phi, \theta, \psi) \mathbf{x}' \quad (35)$$

is given by $\mathbf{R}^T(\phi, \theta, \psi)$, the transpose of the matrix $\mathbf{R}(\phi, \theta, \psi)$ [12]:

$$\begin{aligned} \mathbf{R}^{-1}(\phi, \theta, \psi) &= \mathbf{R}^T(\phi, \theta, \psi) \\ &= \begin{bmatrix} \cos \psi \cos \phi - \cos \theta \sin \phi \sin \psi & -\sin \psi \cos \phi - \cos \theta \sin \phi \cos \psi & \sin \theta \sin \phi \\ \cos \psi \sin \phi + \cos \theta \cos \phi \sin \psi & -\sin \psi \sin \phi + \cos \theta \cos \phi \cos \psi & -\sin \theta \cos \phi \\ \sin \theta \sin \psi & \sin \theta \cos \psi & \cos \theta \end{bmatrix}. \end{aligned} \quad (36)$$

Using Eq. (35), the rescattered EM radiation as projected into the observer's frame (x, y, z) can be expressed as

$$\begin{bmatrix} E_x(\text{scat}) \\ E_y(\text{scat}) \\ E_z(\text{scat}) \end{bmatrix} = \mathbf{R}^{-1}(\phi, \theta, \psi) \begin{bmatrix} E_{x'}(\text{scat}) \\ E_{y'}(\text{scat}) \\ E_{z'}(\text{scat}) \end{bmatrix}, \quad (37)$$

where the quantity $(E_{x'}(\text{scat}), E_{y'}(\text{scat}), E_{z'}(\text{scat}))$ is to be taken from Eqs. (26) – (31), and the values $\{\phi, \theta, \psi\}$ are to be specified for the configuration of the source frame (x', y', z') relative to the observer's frame (x, y, z) . For convenience in Sections II B and III A later, we represent the transformation matrix by

$$\mathbf{R}^{-1}(\phi, \theta, \psi) = \begin{bmatrix} a_{11} & a_{12} & a_{13} \\ a_{21} & a_{22} & a_{23} \\ a_{31} & a_{32} & a_{33} \end{bmatrix}, \quad (38)$$

where a_{ij} ($i, j = 1, 2, 3$) can be directly read off from Eq. (36).

However, as in the case (i) of Figure 2, when the propagation direction of the GWs does not coincide with the line of sight, i.e. $\mathbf{e}'_z \neq \mathbf{e}_z$, the rescattered EM radiation induced by the GWs cannot actually be detected by an observer who is very far away from the source; for $r \gg$ source size in Eqs. (26) – (31). That is, only in the case (ii) of Figure 2, namely, when the propagation direction of the GWs coincides with the line of sight, i.e. $\mathbf{e}'_z = \mathbf{e}_z$, the rescattered EM radiation will be detectable by a distant observer. This will let us fix the direction angles $\{\phi, \theta\} = \{0, 0\}$ and reduce $\mathbf{R}^{-1}(\phi, \theta, \psi)$ to

$$\mathbf{R}^{-1}(0, 0, \psi) = \begin{bmatrix} \cos \psi & -\sin \psi & 0 \\ \sin \psi & \cos \psi & 0 \\ 0 & 0 & 1 \end{bmatrix}, \quad (39)$$

which simply represents the rotation through the polarization-ellipse angle ψ .

B. Stokes parameters for the rescattered EM radiation

In the previous Subsection we have modeled a situation, in which an anisotropic incident radiation is rescattered by a charge being agitated by GWs and the rescattered radiation is indeed induced by the GWs. The charge is set in motion along particular directions by the GWs h_+ or h_\times , and this in fact opens *polarization channels* for the rescattered radiation. For example, a charge being driven to move along the x -axis and the y -axis by GWs h_+ or h_\times will reradiate the reflected light most easily by moving along the same directions. Now, if the incident unpolarized radiation is more intense along one axis than the other, namely, $E_I \neq E_{II}$ in Eqs. (7) and (8), it causes the charge to oscillate more strongly along one axis than the other, i.e. along the x -axis [y -axis] than the y -axis [x -axis], for rescattering (see Figures 1 and 2). Then the radiation emitted by this accelerating charge, which propagates along the third axis, namely, the z -axis, has a *net polarization*. Therefore, the following can be said of the polarization of the CMB induced by primordial GWs: as primordial GWs agitate a charge in the CMB, setting it in periodic, regular motion, the EM radiation rescattered by the charge is partially polarized and this will imprint a characteristic pattern on the light of the CMB. A net *linear* polarization is expected from the rescattered radiation, and it can be shown by determining the *Stokes parameters*. For the two cases of GWs propagating through the CMB, we present the Stokes parameters as below.

1. *Case 1. For GWs propagating along the line of sight*

For the rescattered EM radiation given by (26) - (31), the Stokes parameters can be calculated in a straightforward manner:

$$I_{(\text{case1})} = \langle |E_x(\text{scat})|^2 \rangle + \langle |E_y(\text{scat})|^2 \rangle, \quad (40)$$

$$Q_{(\text{case1})} = \langle |E_x(\text{scat})|^2 \rangle - \langle |E_y(\text{scat})|^2 \rangle, \quad (41)$$

$$U_{(\text{case1})} = \langle E_x(\text{scat})E_y^*(\text{scat}) \rangle + \langle E_x^*(\text{scat})E_y(\text{scat}) \rangle, \quad (42)$$

$$V_{(\text{case1})} = i \left(\langle E_x(\text{scat})E_y^*(\text{scat}) \rangle - \langle E_x^*(\text{scat})E_y(\text{scat}) \rangle \right), \quad (43)$$

where $\langle \rangle$ represents the time average of the enclosed quantity and $*$ denotes the complex conjugate. After some calculations, these parameters turn out to exhibit linear polarization as expected:

$$I_{(\text{case1}) \times}^+ = \frac{q^4 (E_I^2 + E_{II}^2)}{m^2 r^2} \left[1 + h^2 \left(1 + \left(1 - \frac{v_{oz}}{c} \right) \frac{\omega}{\Omega} \right)^2 \right] + \frac{h^2 q^2 (v_{ox}^2 + v_{oy}^2) \left(1 - \frac{v_{oz}}{c} \right)^2 \omega^2}{r^2}, \quad (44)$$

$$Q_{(\text{case1}) \times}^+ = \frac{q^4 (E_{II}^2 - E_I^2)}{m^2 r^2} \left[1 \pm h^2 \left(1 + \left(1 - \frac{v_{oz}}{c} \right) \frac{\omega}{\Omega} \right)^2 \right] \pm \frac{h^2 q^2 (v_{ox}^2 - v_{oy}^2) \left(1 - \frac{v_{oz}}{c} \right)^2 \omega^2}{r^2}, \quad (45)$$

$$U_{(\text{case1}) \times}^+ = 0, \quad (46)$$

$$V_{(\text{case1}) \times}^+ = 0, \quad (47)$$

where the labels $+$ and \times denote the two polarization states of GWs, and the \pm signs on the right-hand side of Eq. (45) follow the order of \times . In these calculations, we have disregarded any contributions from the errors $\mathcal{O}_{I[h]}$, $\mathcal{O}_{II[h]}$ and $\mathcal{O}_{I,II[h]}$: they would be $\mathcal{O}_{[h]}^2 \sim h^2 \times \mathcal{O}_{[0]}^2$ and thus too small to consider.

In Figure 3 is shown the expected spectrum of the characteristic GW amplitude over a broad interval of frequencies [7]. The values of amplitude in this spectrum have been estimated for present time observations, and thus our GW amplitude h in Eqs. (44) and (45) should be distinguished from the values of amplitude for the regime of the CMB anisotropies in the spectrum: our h should be larger than the characteristic amplitude of primordial GWs $\sim 10^{-10}$ as shown in Figure 3. Nevertheless, due to the assumption of linearized gravity as made in Section II A, the order of h^2 should still be regarded as negligibly small, and hence the terms led by h^2 in Eqs. (44) and (45) may be cast off. Taking into consideration the redshift effect from cosmic expansion, our GW frequency ω in Eqs. (44) and (45) should be $\sim 10^3$ times higher than the characteristic frequency for the regime of the CMB anisotropies in the spectrum shown in Figure 3. However, our ω should still be negligibly small (in particular, compared to our EM wave frequency Ω), and hence the terms with ω/Ω and ω^2 in Eqs. (44) and (45) may be cast off too. Therefore, no profiles of our GWs would indeed remain practically in the Stokes parameters (44) - (47). Henceforth we may express the parameters simply in the flat spacetime limit:

$$I_{(\text{case1})} = \frac{q^4 (E_I^2 + E_{II}^2)}{m^2 r^2}, \quad (48)$$

$$Q_{(\text{case1})} = \frac{q^4 (E_{II}^2 - E_I^2)}{m^2 r^2}, \quad (49)$$

$$U_{(\text{case1})} = 0, \quad (50)$$

$$V_{(\text{case1})} = 0, \quad (51)$$

where the expressions are now independent of the polarization states and therefore the signs \times have been dropped.

2. *Case 2. For GWs propagating along an arbitrary direction*

As mentioned in the previous Subsection, our rescattered EM radiation $(E_{x'(\text{scat})}, E_{y'(\text{scat})}, E_{z'(\text{scat})})$ in the source frame takes the same values as Eqs. (26) - (31), except that it is expressed in the coordinates (x', y', z') . However, to

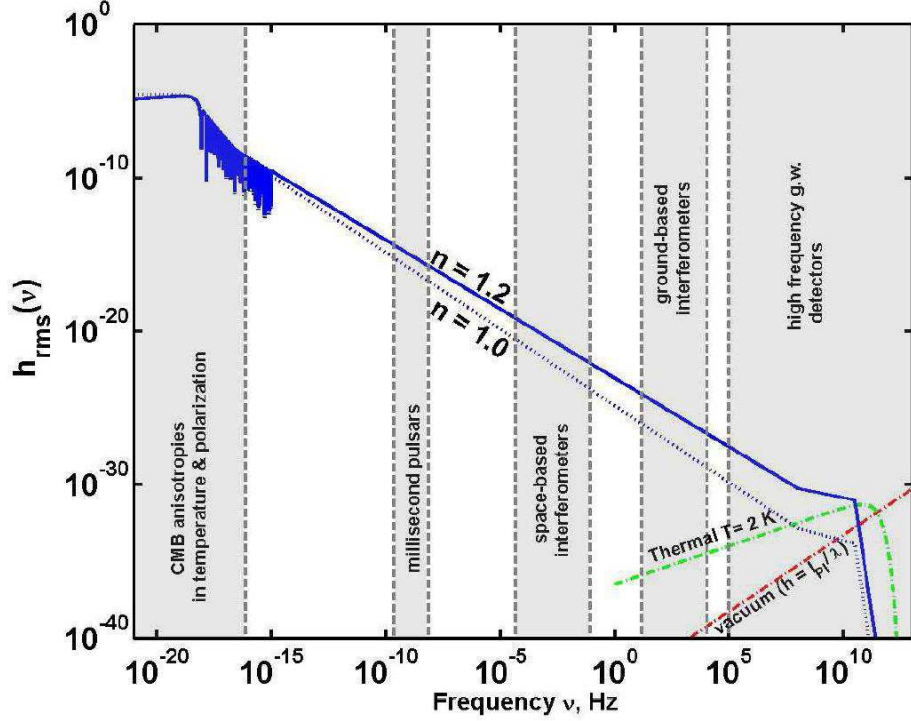


FIG. 3: The expected spectrum of the characteristic GW amplitude h over a broad interval of frequencies. (Credit: The Cardiff Gravitational Physics Group tutorial [7])

compute the Stokes parameters in the observer's frame (x, y, z) , the quantity $(E_{x'(\text{scat})}, E_{y'(\text{scat})}, E_{z'(\text{scat})})$ should be projected into that frame (see Figure 2 for comparison of the observer's frame (x, y, z) and the source frame (x', y', z')). Inserting Eqs. (37) and (38) into Eqs. (40) – (43), after rearranging terms, we have

$$I_{(\text{case2})} = (a_{11}^2 + a_{21}^2) \langle |E_{x'(\text{scat})}|^2 \rangle + (a_{12}^2 + a_{22}^2) \langle |E_{y'(\text{scat})}|^2 \rangle + (a_{11}a_{12} + a_{21}a_{22}) \left(\langle E_{x'(\text{scat})} E_{y'(\text{scat})}^* \rangle + \langle E_{x'(\text{scat})}^* E_{y'(\text{scat})} \rangle \right), \quad (52)$$

$$Q_{(\text{case2})} = (a_{11}^2 - a_{21}^2) \langle |E_{x'(\text{scat})}|^2 \rangle + (a_{12}^2 - a_{22}^2) \langle |E_{y'(\text{scat})}|^2 \rangle + (a_{11}a_{12} - a_{21}a_{22}) \left(\langle E_{x'(\text{scat})} E_{y'(\text{scat})}^* \rangle + \langle E_{x'(\text{scat})}^* E_{y'(\text{scat})} \rangle \right), \quad (53)$$

$$U_{(\text{case2})} = 2a_{11}a_{21} \langle |E_{x'(\text{scat})}|^2 \rangle + 2a_{12}a_{22} \langle |E_{y'(\text{scat})}|^2 \rangle + (a_{11}a_{22} + a_{12}a_{21}) \left(\langle E_{x'(\text{scat})} E_{y'(\text{scat})}^* \rangle + \langle E_{x'(\text{scat})}^* E_{y'(\text{scat})} \rangle \right), \quad (54)$$

$$V_{(\text{case2})} = i(a_{11}a_{22} - a_{12}a_{21}) \left(\langle E_{x'(\text{scat})} E_{y'(\text{scat})}^* \rangle - \langle E_{x'(\text{scat})}^* E_{y'(\text{scat})} \rangle \right), \quad (55)$$

where a_{ij} is read from Eq. (36), and any terms associated with $E_{z'(\text{scat})}$ have been disregarded in the flat spacetime limit: the time average $\langle \rangle$ of these terms would scale as h^2 , which is negligibly small and beyond our measurement limit.

Now, from Eqs. (40) – (43) we may write

$$\langle |E_{x'(\text{scat})}|^2 \rangle = \frac{1}{2} \left(I'_{(\text{case1})} + Q'_{(\text{case1})} \right), \quad (56)$$

$$\langle |E_{y'(\text{scat})}|^2 \rangle = \frac{1}{2} \left(I'_{(\text{case1})} - Q'_{(\text{case1})} \right), \quad (57)$$

$$\langle E_{x'(\text{scat})} E_{y'(\text{scat})}^* \rangle = \frac{1}{2} \left(U'_{(\text{case1})} - iV'_{(\text{case1})} \right), \quad (58)$$

$$\langle E_{x'(\text{scat})}^* E_{y'(\text{scat})} \rangle = \frac{1}{2} \left(U'_{(\text{case1})} + iV'_{(\text{case1})} \right), \quad (59)$$

where the Stokes parameters are defined in the source frame (x', y', z') : however, their values are equal to those in Eqs. (48) – (51) for *Case 1*. Substituting Eqs. (56) – (59) into Eqs. (52) – (55), we establish the following relation:

$$\begin{bmatrix} I_{(\text{case2})} \\ Q_{(\text{case2})} \\ U_{(\text{case2})} \\ V_{(\text{case2})} \end{bmatrix} = \mathbf{L} \begin{bmatrix} I'_{(\text{case1})} \\ Q'_{(\text{case1})} \\ U'_{(\text{case1})} \\ V'_{(\text{case1})} \end{bmatrix}, \quad (60)$$

where

$$\mathbf{L} = \frac{1}{2} \begin{bmatrix} a_{11}^2 + a_{12}^2 + a_{21}^2 + a_{22}^2 & a_{11}^2 - a_{12}^2 + a_{21}^2 - a_{22}^2 & 2(a_{11}a_{12} + a_{21}a_{22}) & 0 \\ a_{11}^2 + a_{12}^2 - a_{21}^2 - a_{22}^2 & a_{11}^2 - a_{12}^2 - a_{21}^2 + a_{22}^2 & 2(a_{11}a_{12} - a_{21}a_{22}) & 0 \\ 2(a_{11}a_{21} + a_{12}a_{22}) & 2(a_{11}a_{21} - a_{12}a_{22}) & 2(a_{11}a_{22} + a_{12}a_{21}) & 0 \\ 0 & 0 & 0 & 2(a_{11}a_{22} - a_{12}a_{21}) \end{bmatrix}, \quad (61)$$

with the values $\{I'_{(\text{case1})}, Q'_{(\text{case1})}, U'_{(\text{case1})}, V'_{(\text{case1})}\}$ to be taken from Eqs. (48) – (51). By means of Eqs. (36) and (38) we can write out Eq. (61):

$$\mathbf{L} = \frac{1}{2} \begin{bmatrix} 1 + \cos^2 \theta & \sin^2 \theta \cos(2\psi) & -\sin^2 \theta \sin(2\psi) & 0 \\ \sin^2 \theta \cos(2\phi) & -2 \cos \theta \sin(2\phi) \sin(2\psi) & -2 \cos \theta \sin(2\phi) \cos(2\psi) & 0 \\ \sin^2 \theta \sin(2\phi) & (1 + \cos^2 \theta) \cos(2\phi) \cos(2\psi) & -(1 + \cos^2 \theta) \cos(2\phi) \sin(2\psi) & 0 \\ 0 & 2 \cos \theta \cos(2\phi) \sin(2\psi) & 2 \cos \theta \cos(2\phi) \cos(2\psi) & 2 \cos \theta \\ & + (1 + \cos^2 \theta) \sin(2\phi) \cos(2\psi) & -(1 + \cos^2 \theta) \sin(2\phi) \sin(2\psi) & 0 \end{bmatrix}. \quad (62)$$

By Eqs. (60) and (62) together with (48) – (51), we can write down explicitly,

$$I_{(\text{case2})} = \frac{1 + \cos^2 \theta}{2} \frac{q^4 (E_{\text{I}}^2 + E_{\text{II}}^2)}{m^2 r^2} + \frac{\sin^2 \theta \cos(2\psi)}{2} \frac{q^4 (E_{\text{II}}^2 - E_{\text{I}}^2)}{m^2 r^2}, \quad (63)$$

$$Q_{(\text{case2})} = \frac{\sin^2 \theta \cos(2\phi)}{2} \frac{q^4 (E_{\text{I}}^2 + E_{\text{II}}^2)}{m^2 r^2} + \left[-\cos \theta \sin(2\phi) \sin(2\psi) + \frac{(1 + \cos^2 \theta) \cos(2\phi) \cos(2\psi)}{2} \right] \frac{q^4 (E_{\text{II}}^2 - E_{\text{I}}^2)}{m^2 r^2} \quad (64)$$

$$U_{(\text{case2})} = \frac{\sin^2 \theta \sin(2\phi)}{2} \frac{q^4 (E_{\text{I}}^2 + E_{\text{II}}^2)}{m^2 r^2} + \left[\cos \theta \cos(2\phi) \sin(2\psi) + \frac{(1 + \cos^2 \theta) \sin(2\phi) \cos(2\psi)}{2} \right] \frac{q^4 (E_{\text{II}}^2 - E_{\text{I}}^2)}{m^2 r^2}, \quad (65)$$

$$V_{(\text{case2})} = 0. \quad (66)$$

These represent the Stokes parameters as computed by an observer as the rescattered EM radiation $(E_{x'(\text{scat})}, E_{y'(\text{scat})}, E_{z'(\text{scat})})$ in the source frame (x', y', z') is projected into the observer's frame (x, y, z) .

However, the argument presented at the end of Section II A 2 suggests that the only physically meaningful transformation from *Case 1* to *Case 2* would be the rotation through the polarization-ellipse angle ψ while fixing the

direction angles $\{\phi, \theta\} = \{0, 0\}$; namely, keeping the propagation direction of GWs aligned with the line of sight, i.e. $\mathbf{e}'_z = \mathbf{e}_z$ (see Figure 2). Then Eqs. (63) – (66) will reduce to

$$I_{(\text{case2})} = \frac{q^4 (E_I^2 + E_{II}^2)}{m^2 r^2}, \quad (67)$$

$$Q_{(\text{case2})} = \cos(2\psi) \frac{q^4 (E_{II}^2 - E_I^2)}{m^2 r^2}, \quad (68)$$

$$U_{(\text{case2})} = \sin(2\psi) \frac{q^4 (E_{II}^2 - E_I^2)}{m^2 r^2} \quad (69)$$

$$V_{(\text{case2})} = 0. \quad (70)$$

In comparison to Eqs. (48) – (51) for *Case 1*, this implies that we have the linear polarization components along the axes rotated from the x -axis and the y -axis by ψ .

III. CMB POLARIZATION OBSERVABLES

A. The Stokes parameters redefined on a sphere and polarization patterns

In the previous Section we have computed the Stokes parameters for the EM radiation rescattered by a charge being shaken by GWs propagating in the CMB. As shown by Eqs. (48) – (51) and (67) – (70), the Stokes parameters exhibit a net linear polarization as desired. However, to analyze the CMB polarization on the sky, it is natural to redefine the Stokes parameters on a sphere such that they can be decomposed into spherical harmonics; to be precise, spin-weighted spherical harmonics as shall be seen later. Below we describe how this is achieved.

First, recall from the previous Section that the Stokes parameters (48) - (51) and (67) - (70) have been computed with respect to $(\mathbf{e}_x, \mathbf{e}_y)$ as the rescattered EM radiation propagates along \mathbf{e}_z in the Cartesian coordinate system (x, y, z) . Now, to redefine the Stokes parameters on a sphere, one should measure them relative to $(\mathbf{e}_\theta, \mathbf{e}_\phi)$ as the rescattered EM radiation propagates along \mathbf{e}_r in the spherical coordinate system (r, θ, ϕ) . This can be achieved via Eq. (32); by rotating the Cartesian frame through the Euler angles $\{\phi, \theta\}$ (direction angles) while fixing the Euler angle $\psi = 0$ (polarization-ellipse angle). This will render the inverse transformation to Eq. (37), which can be equivalently obtained by switching $a_{ij} \leftrightarrow a_{ji}$ (i.e. transpose) and fixing $\psi = 0$ in Eqs. (36) and (38). Further, we find that the inverse transformation to (60) can be obtained by applying the same argument to Eq. (61). That is,

$$\begin{bmatrix} I' \\ Q' \\ U' \\ V' \end{bmatrix} = \mathbf{M} \begin{bmatrix} I \\ Q \\ U \\ V \end{bmatrix}, \quad (71)$$

where

$$\begin{aligned} \mathbf{M} &= \mathbf{L} (a_{ij} \leftrightarrow a_{ji}; \psi = 0) \\ &= \frac{1}{2} \begin{bmatrix} a_{11}^2 + a_{12}^2 + a_{21}^2 + a_{22}^2 & a_{11}^2 + a_{12}^2 - a_{21}^2 - a_{22}^2 & 2(a_{11}a_{21} + a_{12}a_{22}) & 0 \\ a_{11}^2 - a_{12}^2 + a_{21}^2 - a_{22}^2 & a_{11}^2 - a_{12}^2 - a_{21}^2 + a_{22}^2 & 2(a_{11}a_{21} - a_{12}a_{22}) & 0 \\ 2(a_{11}a_{12} + a_{21}a_{22}) & 2(a_{11}a_{12} - a_{21}a_{22}) & 2(a_{11}a_{22} + a_{12}a_{21}) & 0 \\ 0 & 0 & 0 & 2(a_{11}a_{22} - a_{12}a_{21}) \end{bmatrix}_{\psi=0} \\ &= \frac{1}{2} \begin{bmatrix} 1 + \cos^2 \theta & \sin^2 \theta \cos(2\phi) & \sin^2 \theta \sin(2\phi) & 0 \\ \sin^2 \theta & (1 + \cos^2 \theta) \cos(2\phi) & (1 + \cos^2 \theta) \sin(2\phi) & 0 \\ 0 & -2 \cos \theta \sin(2\phi) & 2 \cos \theta \cos(2\phi) & 0 \\ 0 & 0 & 0 & 2 \cos \theta \end{bmatrix}, \quad (72) \end{aligned}$$

with a_{ij} identified from Eqs. (36) and (38). Here Eq. (71) means that the Stokes parameters $\{I', Q', U', V'\}$ (in the spherical coordinate system) are equal to the values of the Stokes parameters $\{I, Q, U, V\}$ (in the Cartesian coordinate

system) as measured relative to $(\mathbf{e}_\theta, \mathbf{e}_\phi)$: the Stokes parameters $\{I', Q', U', V'\}$ are functions of spherical polar angles $\{\phi, \theta\}$ while the Stokes parameters $\{I, Q, U, V\}$ are constant evaluated values in the Cartesian frame, given by Eqs. (48) – (51) or (67) – (70). Hereafter, for notational convenience, we drop the sign ' from $\{I', Q', U', V'\}$ on the left-hand side of Eq. (71) but put the subscript $_c$ (to stand for 'constant') in $\{I, Q, U, V\}$ on the right-hand side. Then we may rewrite Eq. (71) as

$$\begin{bmatrix} I \\ Q \\ U \\ V \end{bmatrix} = \frac{3}{4} \begin{bmatrix} 1 + \cos^2 \theta & \sin^2 \theta \cos(2\phi) & \sin^2 \theta \sin(2\phi) & 0 \\ \sin^2 \theta & (1 + \cos^2 \theta) \cos(2\phi) & (1 + \cos^2 \theta) \sin(2\phi) & 0 \\ 0 & -2 \cos \theta \sin(2\phi) & 2 \cos \theta \cos(2\phi) & 0 \\ 0 & 0 & 0 & 2 \cos \theta \end{bmatrix} \begin{bmatrix} I_c \\ Q_c \\ U_c \\ V_c \end{bmatrix}, \quad (73)$$

where $\{I_c, Q_c, U_c, V_c\}$ refer to Eqs. (48) – (51) or (67) – (70), and the factor $1/2$ from the matrix (72) has been readjusted to $3/4$ for normalization [8, 13]; such that the scattered intensity integrated over all directions, $0 \leq \phi < 2\pi$, $0 \leq \theta < \pi$ equal the intensity of the incoming radiation.

To study the linear polarization of the CMB, we examine only Q and U among the Stokes parameters. From Eq. (73) the combinations of the two parameters turn out to be

$$\begin{aligned} Q \pm iU &= \frac{3}{4} I_c \sin^2 \theta + Q_c \left[\frac{3}{4} (1 + \cos^2 \theta) \cos(2\phi) \mp i \frac{3}{2} \cos \theta \sin(2\phi) \right] \\ &+ U_c \left[\frac{3}{4} (1 + \cos^2 \theta) \sin(2\phi) \pm i \frac{3}{2} \cos \theta \cos(2\phi) \right]. \end{aligned} \quad (74)$$

Or we can put this in the representation,

$$Q \pm iU = \sqrt{\frac{6\pi}{5}} I_c {}_{\pm 2}Y_2^0(\theta, \phi) + \sqrt{\frac{9\pi}{5}} (Q_c - iU_c) {}_{\pm 2}Y_2^2(\theta, \phi) + \sqrt{\frac{9\pi}{5}} (Q_c + iU_c) {}_{\pm 2}Y_2^{-2}(\theta, \phi), \quad (75)$$

where ${}_{\pm s}Y_\ell^m$ represent the spin-weighted spherical harmonics of spin $\pm s$ [22]. This clearly shows that $Q \pm iU$ are spin ± 2 quantities.

However, from Eqs. (60) and (62) we can express $\{I_c, Q_c, U_c, V_c\}$ in the most general case for observation:

$$I_c = I_o, \quad (76)$$

$$Q_c = \cos(2\psi_o) Q_o - \sin(2\psi_o) U_o, \quad (77)$$

$$U_c = \sin(2\psi_o) Q_o + \cos(2\psi_o) U_o, \quad (78)$$

$$V_c = V_o, \quad (79)$$

where ψ_o denotes the value of polarization-ellipse angle, by which the source frame (x', y', z') is rotated from the observer's frame (x, y, z) with respect to the z -axis while keeping $\mathbf{e}'_z = \mathbf{e}_z$ (see Figure 2 for comparison of the two frames), and

$$I_o \equiv I_{(\text{case1})} = \frac{q^4 (E_I^2 + E_{II}^2)}{m^2 r^2}, \quad (80)$$

$$Q_o \equiv Q_{(\text{case1})} = \frac{q^4 (E_{II}^2 - E_I^2)}{m^2 r^2}, \quad (81)$$

$$U_o \equiv U_{(\text{case1})} = 0, \quad (82)$$

$$V_o \equiv V_{(\text{case1})} = 0, \quad (83)$$

by Eqs. (48) – (51). In the limit $\psi_o \rightarrow 0$, we have $\{I_c, Q_c, U_c, V_c\} \rightarrow \{I_o, Q_o, U_o, V_o\}$. Inserting Eqs. (76) – (79) into Eq. (74), we may rewrite

$$\begin{aligned} Q \pm iU &= \frac{3}{4} I_o \sin^2 \theta \\ &+ \frac{3}{4} Q_o \left[(1 + \cos^2 \theta) \cos(2(\phi - \psi_o)) \mp i 2 \cos \theta \sin(2(\phi - \psi_o)) \right]. \end{aligned} \quad (84)$$

Here the term $\frac{3}{4}I_o \sin^2 \theta$ refers to the total intensity of radiation and does not concern polarization. Therefore, we may remove this and redefine

$$\bar{Q} \pm i\bar{U} = \frac{3}{4}Q_o [(1 + \cos^2 \theta) \cos(2(\phi - \psi_o)) \mp i2 \cos \theta \sin(2(\phi - \psi_o))]. \quad (85)$$

Or we can represent this using the spin-weighted spherical harmonics,

$$\bar{Q} \pm i\bar{U} = \sqrt{\frac{9\pi}{5}}Q_o [\pm 2Y_2^2(\theta, \phi - \psi_o) + \pm 2Y_2^{-2}(\theta, \phi - \psi_o)]. \quad (86)$$

By means of Eqs. (85) or (86), we can illustrate polarization patterns; namely, ‘‘electric’’ E-mode and ‘‘magnetic’’ B-mode patterns [15]. The polarization amplitude and angle clockwise from the north pole (at $\theta = 0$) are defined to represent E-modes, and B-modes can be represented by rotating the E-modes by 45° :

$$\begin{aligned} \text{Amplitude} &= \sqrt{\bar{Q}^2 + \bar{U}^2} \\ &= \frac{3}{4}|Q_o| \left\{ [(1 + \cos^2 \theta) \cos(2(\phi - \psi_o))]^2 + [-2 \cos \theta \sin(2(\phi - \psi_o))]^2 \right\}^{1/2}, \end{aligned} \quad (87)$$

$$\begin{aligned} \text{Angle (E-modes)} &= \frac{1}{2} \arctan\left(\frac{\bar{U}}{\bar{Q}}\right) \\ &= \frac{1}{2} \arctan\left(\frac{-2 \cos \theta \tan(2(\phi - \psi_o))}{1 + \cos^2 \theta}\right), \end{aligned} \quad (88)$$

$$\text{Angle (B-modes)} = \text{Angle (E-modes)} + \frac{\pi}{4}, \quad (89)$$

with Q_o given by Eq. (81). Regarding the definitions of E-modes/B-modes, we followed [15]. Eqs. (88) and (89) refer to the angles for E-modes/B-modes derived from the ‘spin ± 2 ’ quantity as given by Eq. (86); this should be distinguished from the later case of Eqs. (103) and (104) which refer to the angles for E-modes/B-modes derived from the ‘spin 0’ quantity as given by Eq. (101).

Graphic representation 1

The E-mode and B-mode patterns based on Eqs. (87), (88) and (89) above are graphically represented in Figure 4; given the polarization-ellipse angle ψ_o , which determines the orientation of the source frame (x', y', z') with respect to the observer’s frame (x, y, z) (see Figure 2 for comparison of the two frames). The patterns may be characterized as follows.

(i) Figures 4a (E-modes) and 4b (B-modes) with $\psi_o = 0$:

The source frame (x', y', z') coincides with the observer’s frame (x, y, z) , and therefore the rescattered EM radiation is received by the observer with its full intensity and the maximum polarization effect. The E-modes and B-modes exhibit regular gradient-like and curl-like patterns, respectively.

(ii) Figures 4c (E-modes) and 4d (B-modes) with $\psi_o = \pi/4$:

The source frame (x', y', z') is rotated by $\pi/4$ from the observer’s frame (x, y, z) with respect to the z -axis. The E-modes and B-modes exhibit the same patterns as in case (i) except that the both patterns are now shifted along ϕ by $\psi_o = \pi/4$; therefore physically equivalent to case (i).

B. Plane wave modulation of polarization patterns

The E-mode and B-mode patterns of polarization in the previous Subsection represent the local signature from scattering over the sphere. However, in real-world observations the polarization patterns on the sky are not simply the local signature from scattering but are modulated by plane wave fluctuations on the last scattering surface. The

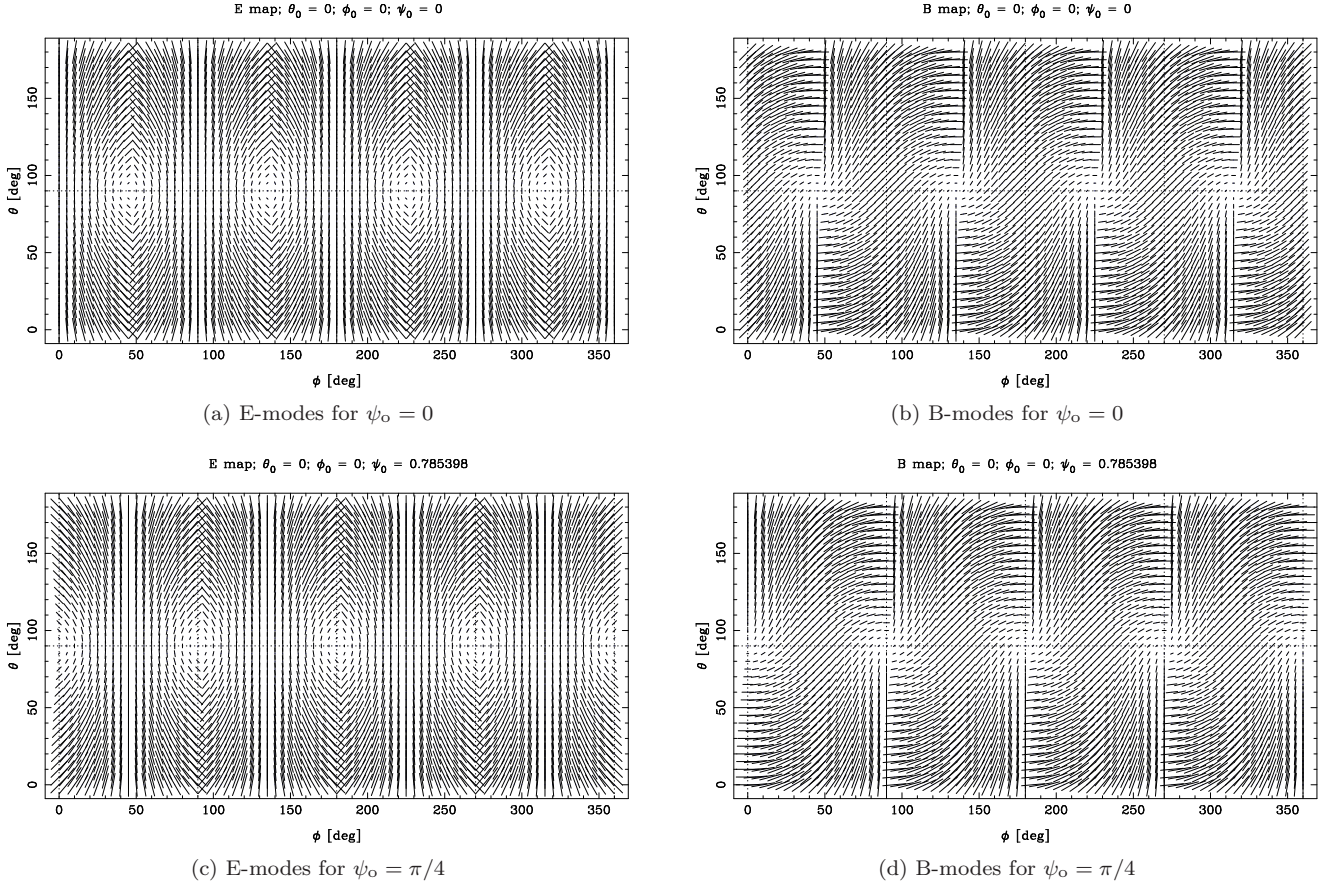


FIG. 4: The E-mode and B-mode patterns of polarization given the polarization-ellipse angle ψ_0 .

plane wave modulation changes the amplitude, sign and angular structure of the polarization but not its nature: that is, it does not mix Q and U [15].

The quantities given by Eqs. (85) or (86) have a direct association with physical observables, namely, Stokes parameters, and from them we can illustrate the polarization patterns as was done at the end of the previous Subsection. However, as can be seen from Eq. (86), these are spin ± 2 quantities, and it would be desirable to derive rotationally invariant spin 0 quantities out of them [17, 18, 29]. Now, we define

$$\tilde{Q} \pm i\tilde{U} \equiv (\bar{Q} \pm i\bar{U}) \exp(i\mathbf{k} \cdot \mathbf{r}) = (\bar{Q} \pm i\bar{U}) \exp(i\rho \cos \theta); \quad \rho \equiv kr, \quad (90)$$

where $\mathbf{k} = k\mathbf{e}_z$ and $\mathbf{r} = r\mathbf{e}_r$, with k denoting the wave number and r the comoving distance to the last scattering surface, and $\exp(i\mathbf{k} \cdot \mathbf{r}) = \exp(ikr \cos \theta) = \exp(i\rho \cos \theta)$ represents the plane wave projected into the spherical sky [16]. From this we can construct the following scalar quantities [17, 18, 29]:

$$\tilde{E} \equiv -\frac{1}{2} \left[\bar{\partial}^2 (\tilde{Q} + i\tilde{U}) + \partial^2 (\tilde{Q} - i\tilde{U}) \right], \quad (91)$$

$$\tilde{B} \equiv \frac{i}{2} \left[\bar{\partial}^2 (\tilde{Q} + i\tilde{U}) - \partial^2 (\tilde{Q} - i\tilde{U}) \right], \quad (92)$$

where the spin raising and lowering operators are defined as

$$\bar{\partial}_s f(\theta, \phi) = -(\sin \theta)^s \left(\frac{\partial}{\partial \theta} + i \csc \theta \frac{\partial}{\partial \phi} \right) (\sin \theta)^{-s} f(\theta, \phi), \quad (93)$$

$$\partial_s f(\theta, \phi) = -(\sin \theta)^{-s} \left(\frac{\partial}{\partial \theta} - i \csc \theta \frac{\partial}{\partial \phi} \right) (\sin \theta)^s f(\theta, \phi), \quad (94)$$

for an arbitrary spin s quantity ${}_s f(\theta, \phi)$. Substituting Eq. (85) into Eq. (90), and subsequently Eq. (90) into Eqs. (91) and (92), we obtain

$$\tilde{E} = \frac{3}{4} Q_o \sin^2 \theta [\rho^2 (1 + \cos^2 \theta) - 12 - 8i\rho \cos \theta] \cos(2(\phi - \psi_o)) \exp(i\rho \cos \theta), \quad (95)$$

$$\tilde{B} = \frac{3}{2} Q_o \sin^2 \theta (-\rho^2 \cos \theta + 4i\rho) \sin(2(\phi - \psi_o)) \exp(i\rho \cos \theta). \quad (96)$$

Here we note that the spin 0 quantity $\exp(i\rho \cos \theta)$ is a common phase factor for the complex quantities \tilde{E} and \tilde{B} . With this factor suppressed, the relative phase between the two complex quantities still remains the same. Then we may define

$$\bar{E} \equiv \tilde{E} \exp(-i\rho \cos \theta), \quad (97)$$

$$\bar{B} \equiv \tilde{B} \exp(-i\rho \cos \theta), \quad (98)$$

such that their combinations are

$$\bar{E} + i\bar{B} = (\tilde{E} + i\tilde{B}) \exp(-i\rho \cos \theta) = -\bar{\partial}^2 (\tilde{Q} + i\tilde{U}) \exp(-i\rho \cos \theta), \quad (99)$$

$$\bar{E} - i\bar{B} = (\tilde{E} - i\tilde{B}) \exp(-i\rho \cos \theta) = -\bar{\partial}^2 (\tilde{Q} - i\tilde{U}) \exp(-i\rho \cos \theta), \quad (100)$$

by means of Eqs. (91) and (92). By Eqs. (95) and (96) these read

$$\begin{aligned} \bar{E} \pm i\bar{B} &= \frac{3}{4} Q_o \sin^2 \theta \{ [\rho^2 (1 + \cos^2 \theta) - 12] \cos(2(\phi - \psi_o)) \mp 8\rho \sin(2(\phi - \psi_o)) \\ &\quad + i \cos \theta [-8\rho \cos(2(\phi - \psi_o)) \mp 2\rho^2 \sin(2(\phi - \psi_o))] \}. \end{aligned} \quad (101)$$

Here we note that $\bar{E} - i\bar{B}$ can be obtained by changing $\phi - \psi_o \rightarrow -(\phi - \psi_o)$ in $\bar{E} + i\bar{B}$. This means that $\bar{E} - i\bar{B}$ is the reflection of $\bar{E} + i\bar{B}$ about $\phi = \psi_o$. Therefore, $\bar{E} + i\bar{B}$ and $\bar{E} - i\bar{B}$ lead to physically equivalent representations: they produce patterns which are simply mirror images of each other³.

We choose $\bar{E} + i\bar{B}$ for our representation of polarization patterns. Similarly as in the previous Subsection, one can illustrate the E-mode and B-mode polarization patterns by means of Eq. (101). We represent E-modes by the polarization amplitude and angle clockwise from the north pole (at $\theta = 0$), and B-modes by rotating the E-modes by 45°:

$$\text{Amplitude} = \sqrt{[\Re(\bar{E} + i\bar{B})]^2 + [\Im(\bar{E} + i\bar{B})]^2}, \quad (102)$$

$$\text{Angle (E-modes)} = \frac{1}{2} \arctan \left(\frac{\Im(\bar{E} + i\bar{B})}{\Re(\bar{E} + i\bar{B})} \right), \quad (103)$$

$$\text{Angle (B-modes)} = \text{Angle (E-modes)} + \frac{\pi}{4}, \quad (104)$$

where

$$\Re(\bar{E} + i\bar{B}) = \frac{3}{4} Q_o \sin^2 \theta \{ [\rho^2 (1 + \cos^2 \theta) - 12] \cos(2(\phi - \psi_o)) - 8\rho \sin(2(\phi - \psi_o)) \}, \quad (105)$$

$$\Im(\bar{E} + i\bar{B}) = -\frac{3}{2} Q_o \sin^2 \theta \cos \theta [4\rho \cos(2(\phi - \psi_o)) + \rho^2 \sin(2(\phi - \psi_o))], \quad (106)$$

with Q_o given by Eq. (81).

In particular, for $\rho \gg 1$, which corresponds to small angular scales, the representations of E-modes and B-modes tend to

$$\text{Amplitude} = \frac{3}{4} |Q_o| \rho^2 \sin^2 \theta \left\{ [(1 + \cos^2 \theta) \cos(2(\phi - \psi_o))]^2 + [-2 \cos \theta \sin(2(\phi - \psi_o))]^2 \right\}^{1/2}, \quad (107)$$

³ The same argument applies to $\bar{Q} + i\bar{U}$ and $\bar{Q} - i\bar{U}$ due to Eq. (85).

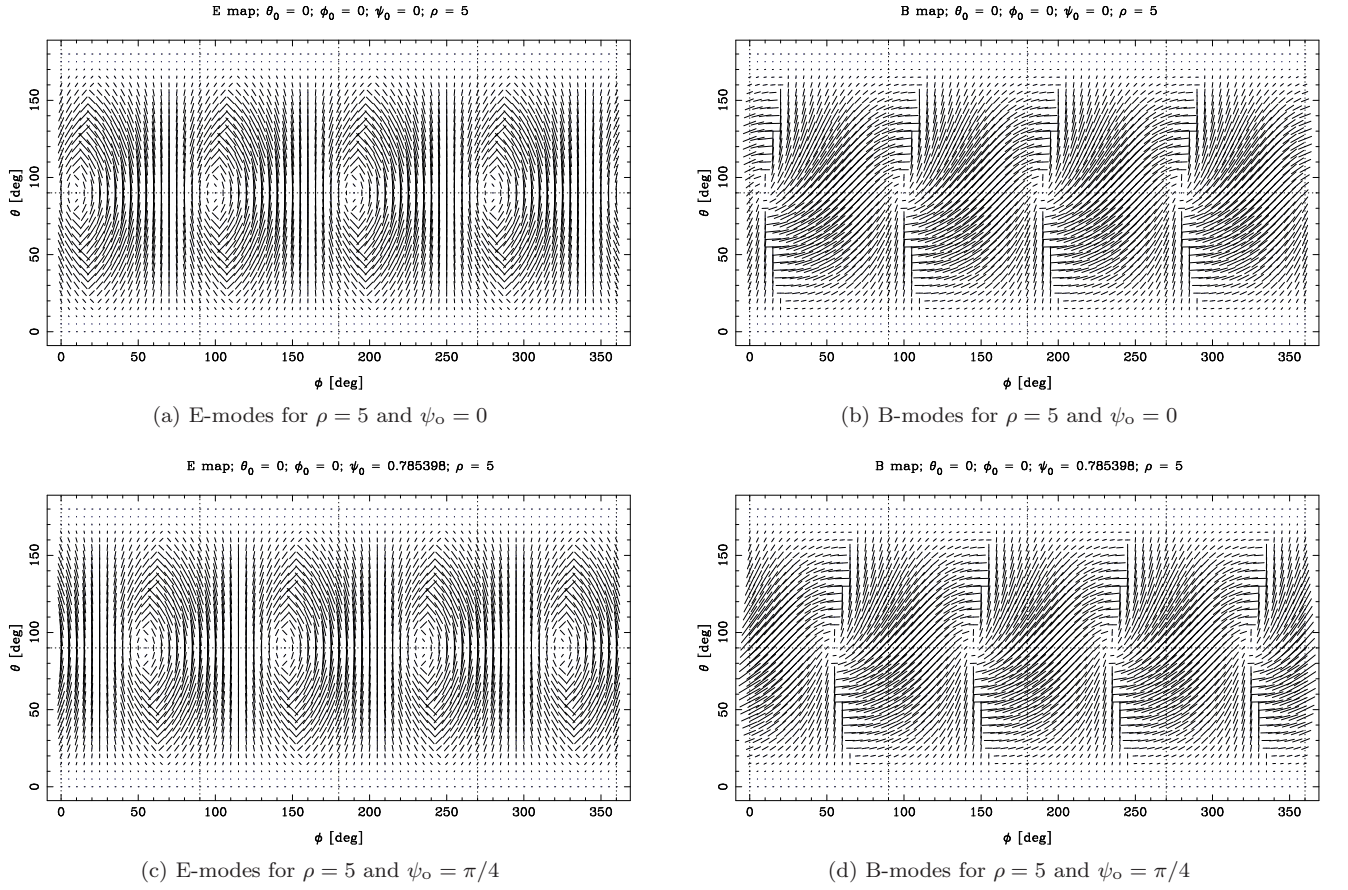


FIG. 5: The E-mode and B-mode patterns of polarization for $\rho = 5$ and the polarization-ellipse angle ψ_o .

$$\text{Angle (E-modes)} = \frac{1}{2} \arctan \left(\frac{-2 \cos \theta \tan (2(\phi - \psi_o))}{(1 + \cos^2 \theta)} \right), \quad (108)$$

$$\text{Angle (B-modes)} = \text{Angle (E-modes)} + \frac{\pi}{4}. \quad (109)$$

We note that these scale to the spin 2 representations given by Eqs. (87), (88) and (89), apart from the factor $\rho^2 \sin^2 \theta$ in the amplitude [9].

Graphic representation 2

The E-mode and B-mode patterns based on Eqs. (102), (103) and (104) above are graphically represented in Figures 5, 6 and 7; with the dimensionless parameter ρ , which defines the plane wave projection into the spherical sky (i.e. $\exp(\mathbf{i}\mathbf{k} \cdot \mathbf{r}) = \exp(ikr \cos \theta) = \exp(i\rho \cos \theta)$) and with the polarization-ellipse angle ψ_o , which determines the orientation of the source frame (x', y', z') with respect to the observer's frame (x, y, z) (see Figure 2 for comparison of the two frames). Given different values of ρ and ψ_o , the patterns may be characterized as follows.

1. In Figure 5

(i') Figures 5a (E-modes) and 5b (B-modes) with $\rho = 5$, $\psi_o = 0$:

The source frame (x', y', z') coincides with the observer's frame (x, y, z) , and therefore the rescattered EM radiation is received by the observer with its full intensity and the maximum polarization effect. The E-modes and B-modes exhibit gradient-like and curl-like patterns but with broken symmetric and anti-symmetric images in each quadrant for ϕ , respectively. This is caused by the plane wave modulation at *long* wavelengths or at *small* comoving distances to the last scattering surface; due to Eqs. (103) and (104) with $\rho = 2\pi r/\lambda$.

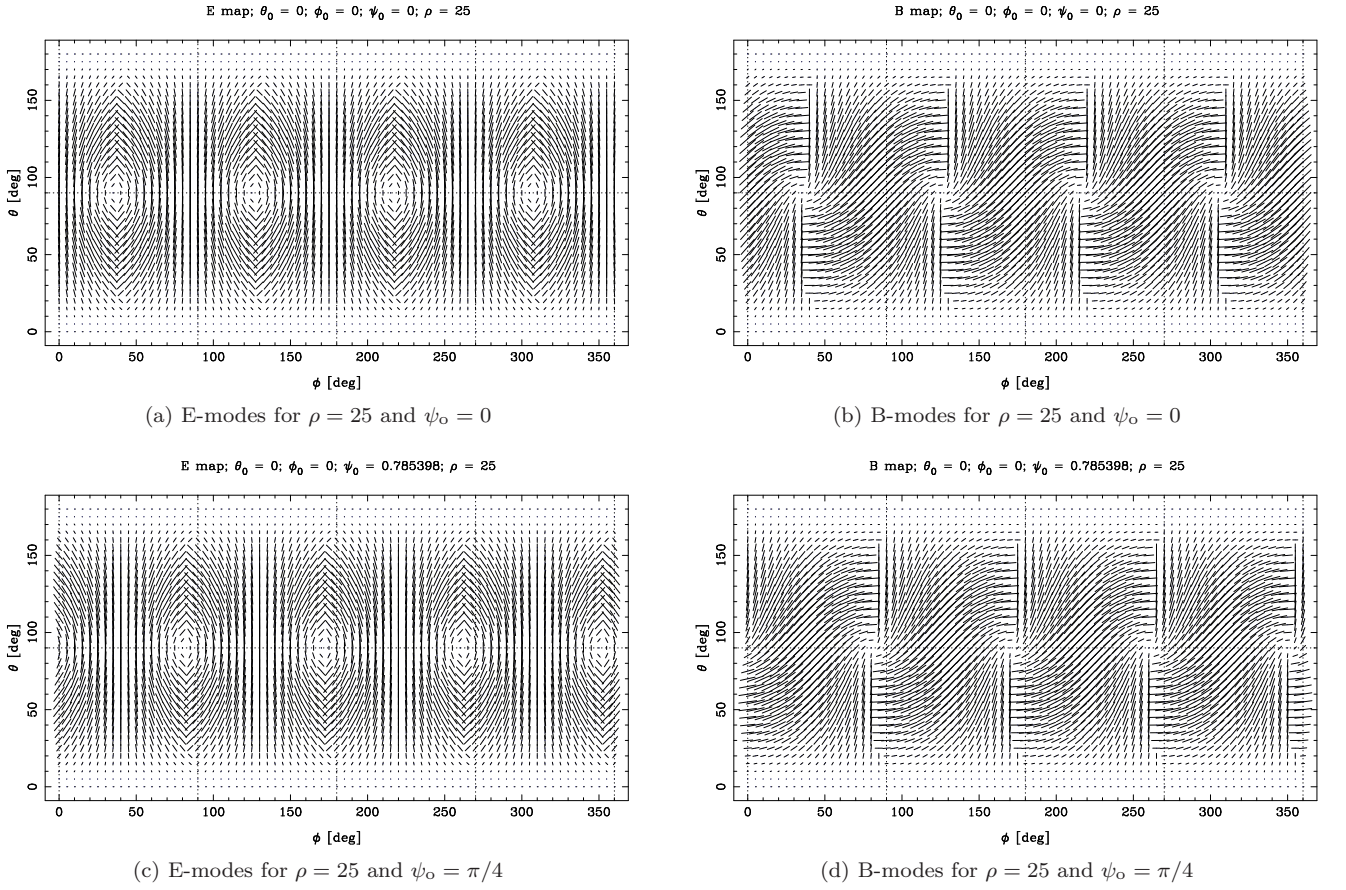


FIG. 6: The E-mode and B-mode patterns of polarization for $\rho = 25$ and the polarization-ellipse angle ψ_0 .

(ii') Figures 5c (E-modes) and 5d (B-modes) with $\rho = 5$, $\psi_0 = \pi/4$:

The source frame (x', y', z') is rotated by $\pi/4$ from the observer's frame (x, y, z) with respect to the z -axis. The E-modes and B-modes exhibit the same patterns as in case (i') except that the both patterns are now shifted along ϕ by $\psi_0 = \pi/4$; therefore physically equivalent to case (i').

2. In Figure 6

(i'') Figures 6a (E-modes) and 6b (B-modes) with $\rho = 25$, $\psi_0 = 0$:

The source frame (x', y', z') coincides with the observer's frame (x, y, z) , and therefore the rescattered EM radiation is received by the observer with its full intensity and the maximum polarization effect. The E-modes and B-modes exhibit gradient-like and curl-like patterns but with broken symmetric and anti-symmetric images in each quadrant for ϕ , respectively; however, less broken than in case (i'). This is caused by the plane wave modulation at *medium* wavelengths or at *medium* comoving distances to the last scattering surface; due to Eqs. (103) and (104) with $\rho = 2\pi r/\lambda$.

(ii'') Figures 6c (E-modes) and 6d (B-modes) with $\rho = 25$, $\psi_0 = \pi/4$:

The source frame (x', y', z') is rotated by $\pi/4$ from the observer's frame (x, y, z) with respect to the z -axis. The E-modes and B-modes exhibit the same patterns as in case (i'') except that the both patterns are now shifted along ϕ by $\psi_0 = \pi/4$; therefore physically equivalent to case (i'').

3. In Figure 7

(i''') Figures 7a (E-modes) and 7b (B-modes) with $\rho = 125$, $\psi_0 = 0$:

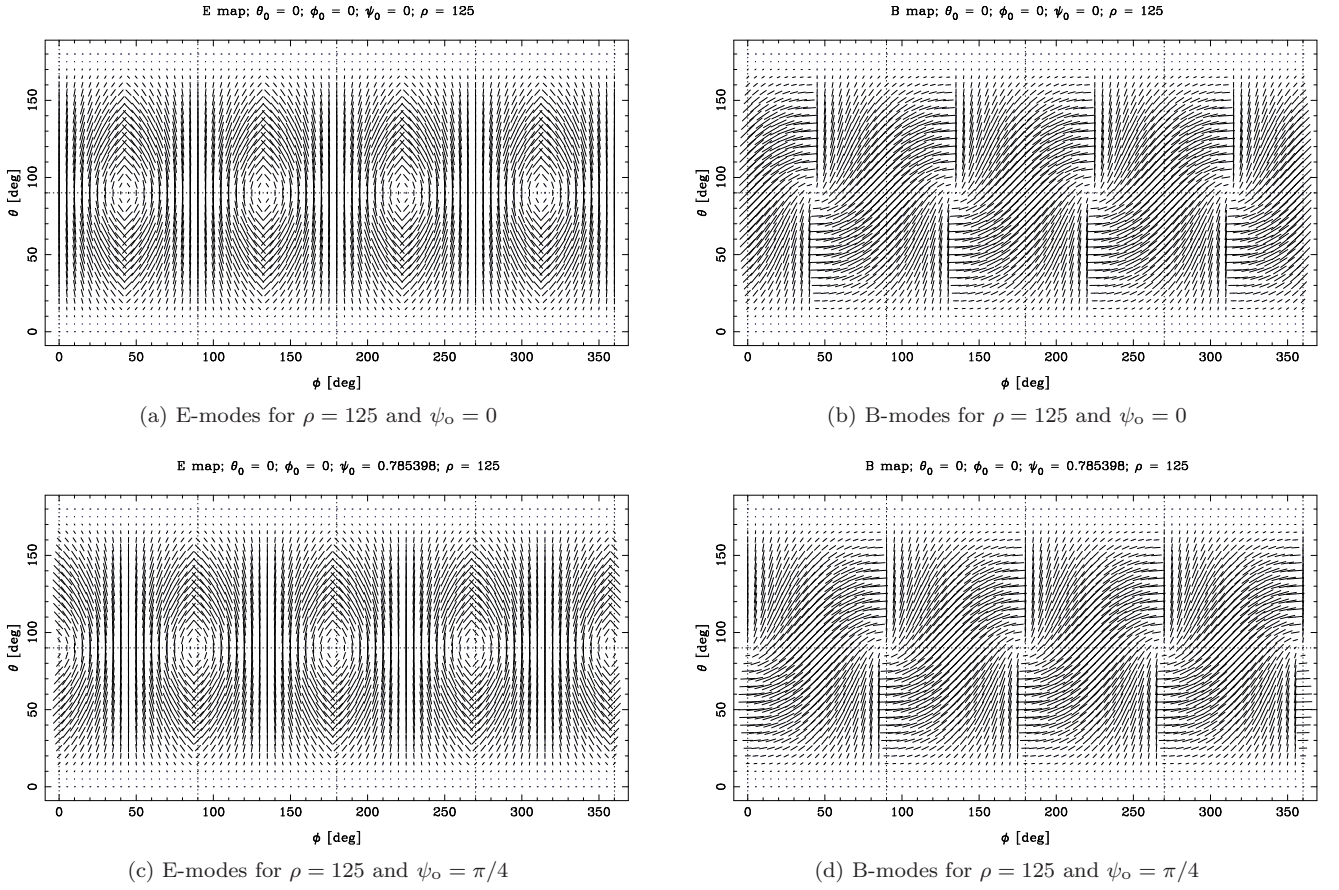


FIG. 7: The E-mode and B-mode patterns of polarization for $\rho = 125$ and the polarization-ellipse angle ψ_o .

The source frame (x', y', z') coincides with the observer's frame (x, y, z) , and therefore the rescattered EM radiation is received by the observer with its full intensity and the maximum polarization effect. The E-modes and B-modes exhibit *regular* gradient-like and curl-like patterns with proper symmetric and anti-symmetric images in each quadrant for ϕ , respectively. This is caused by the plane wave modulation at *short* wavelengths or at *large* comoving distances to the last scattering surface; due to Eqs. (103) and (104) with $\rho = 2\pi r/\lambda$.

(ii''') Figures 7c (E-modes) and 7d (B-modes) with $\rho = 125$, $\psi_o = \pi/4$:

The source frame (x', y', z') is rotated by $\pi/4$ from the observer's frame (x, y, z) with respect to the z -axis. The E-modes and B-modes exhibit the same patterns as in case (i''') except that the both patterns are now shifted along ϕ by $\psi_o = \pi/4$; therefore physically equivalent to case (i''').

Cases (i') and (i'') from Figures 5 and 6 show that the broken symmetric and anti-symmetric images in the E-mode and B-mode patterns are due to the plane wave modulation at *long* to *medium* wavelengths or at *small* to *medium* comoving distances to the last scattering surface, which corresponds to small to medium ρ . However, case (i''') from Figure 7 shows that the E-mode and B-mode patterns take proper symmetric and anti-symmetric images, respectively, with the plane wave modulation at *short* wavelengths or at *large* comoving distances to the last scattering surface, which corresponds to large ρ : in fact, these patterns should be equivalent to the ones to be produced via Eqs. (107), (108) and (109) in the limit $\rho \gg 1$. While the plane wave modulation affects the symmetric and anti-symmetric properties of the E-modes and B-modes, depending on the size of ρ , it does not change the periodicity of the patterns in ϕ (i.e. $\pi/2$): in both the E-mode and B-mode patterns, four identical images are produced over $0 \leq \phi < 2\pi$, one in each of the four quadrants.

IV. DISCUSSION AND CONCLUSIONS

We present an analysis of an apparently as yet overlooked effect in the interaction between (primordial) GWs and individual electric charges. We computed the Stokes parameters for the EM radiation rescattered by a charge that is forced into oscillatory motion by GWs propagating through the CMB plasma: as shown by Eqs. (48) – (51) and (67) – (70) in Section II B, the Stokes parameters exhibit a net linear polarization – as expected. The GWs *open polarization channels* for the rescattered radiation by setting a charge in motion along particular directions. In other words, the GWs provide for polarization in the photon-electron scattering by agitating a charge along particular directions. Taking the $\mathcal{O}(h)$ terms into consideration, the resulting contribution to our Stokes parameters will be as shown in Eqs. (44) – (47), which is $\mathcal{O}(h^2)$. In our analysis, due to the assumption of linearized gravity in Section II A, $\mathcal{O}(h^2)$ would be considered as very small, and therefore the terms of this order may be disregarded for the final expressions of the Stokes parameters as in Eqs. (48) – (51). However, until we are able to estimate how large or small the strain h is in the CMB regime [unlike its estimates for present time observations as in Figure 3], it is not clear whether the negligence of $\mathcal{O}(h^2)$ will make any significant difference (or not) in our final E-mode/B-mode maps. Our analysis is presently limited to modeling single-electron scattering; accordingly, we are not yet able to provide a reliable estimate of the amount of polarized flux to be expected. Evidently, reliable amplitude estimates will be crucial for attempts to observe the effect we describe in this study; current B-mode polarization studies have sensitivities of about $0.3 \mu\text{K}\sqrt{s}$ (in CMB temperature units, using BICEP2 as benchmark; [2]).

If our measurement were indeed sensitive enough to tell the values of the strain h and the frequency ω of the GWs in the CMB regime, then we should rather express our Stokes parameters using Eqs. (44) – (47). This way, we would be able to see the properties of the GWs directly from our E-mode/B-mode polarization maps through the Stokes parameters. In particular, the second parameter Q would take different values, depending on the GW polarization states, $+$ and \times , while the first parameter I would be the same regardless of the states. This implies that the linear polarization of our CMB radiation would be quantified differently, depending on the GW polarization states. That is, $Q_+ = Q_o + \mathcal{O}(h^2)$ and $Q_\times = Q_o - \mathcal{O}(h^2)$ while $I_+ = I_\times = I_o + \mathcal{O}(h^2)$, and therefore we find the ratios, $Q_+/I_+ \neq Q_\times/I_\times$. This means that the GW-induced polarization should show this distinctive feature, which will distinguish itself from other degenerate cases, where polarization could possibly have been induced from non-GW sources.

In order to analyze the CMB polarization on the sky, we have redefined the Stokes parameters on a sphere such that their representations can be expressed as spin-weighted spherical harmonics; namely, spin ± 2 quantities. The representations yield the two polarization patterns, “electric” E-mode and “magnetic” B-mode patterns [15]. They are constructed by means of Eqs. (87), (88) and (89), and graphically represented in Figure 4 (see **Graphic representations 1**) in Section III A. While these patterns represent the local signature from scattering over the sphere, in real-world observations, the polarization patterns on the sky are not simply the local signature from scattering but are modulated by plane wave fluctuations on the last scattering surface [15]. Thus we have modified the representations of the Stokes parameters such that they contain the properties of the plane wave projected into the spherical sky. The modified representations are spin 0 quantities, and they also yield the E-mode and B-mode polarization patterns [17, 18, 29]. They are constructed by means of Eqs. (102), (103) and (104), and graphically represented in Figures 5, 6 and 7 (see **Graphic representations 2**) in Section III B; with different conditions of the plane wave projection into the spherical sky.

Overall, GWs can generate the gradient- and curl-like E- and B-modes as expected. Even though, notable differences between **Graphic representations 1** and **2** are observed due to the plane wave modulation; parameterized by ρ , which defines the plane wave projection into the spherical sky. With small to medium ρ , which corresponds to the plane wave modulation at *long* to *medium* wavelengths or at *small* to *medium* comoving distances to the last scattering surface, the E-modes and B-modes show broken symmetric and anti-symmetric patterns, respectively in **Graphic representations 2**. However, with large ρ , which corresponds to the plane wave modulation at *short* wavelengths or at *large* comoving distances to the last scattering surface, the E-modes and B-modes take proper symmetric and anti-symmetric patterns. In fact, in the limit $\rho \gg 1$, the E-modes and B-modes in **Graphic representations 2** scale to their counterparts in **Graphic representations 1**, apart from the factor $\rho^2 \sin^2 \theta$ in the amplitude [9]. In both **Graphic representations 1** and **2**, however, the periodicity of the patterns in ϕ for the E-modes and B-modes

remains the same, i.e. $\pi/2$.

In this work we have restricted our attention to the case of a single charged particle under the influence of GWs passing through the CMB. We have investigated how the EM radiation is rescattered by the charge being agitated by the GWs and how the rescattered radiation becomes polarized in the CMB. More realistic astronomical scenarios, however, would involve multiple charged particles interacting with each other. At the same time, as we assume that our universe was expanding during the epoch of reionization, the interaction between the particles would be significantly affected by the scale factor of the expanding universe. Therefore, to handle a situation with the interaction properly, the motion of the particles should be described in the spacetime geometry which is prescribed by the perturbed Friedmann-Robertson-Walker metric rather than by the perturbed flat spacetime metric. Unlike the case of a single particle, dynamic evolution of the multiple particles in this setup should be treated statistically, e.g. using the Boltzmann equation [16, 17, 29]. Likewise, astrophysically realistic CMB polarization maps – which we do not provide here – result from convolution of the patterns caused by single-particle interaction with the density distribution of the CMB plasma. Furthermore, we do not yet present power spectra in this study. Following [16], we can determine the ℓ -mode expressions for the power spectra out of Eqs. (86) and (90) – (92) by means of the Clebsch-Gordan relation. With these we will be able to estimate the E-mode/B-mode contributions in a quantitative manner as shown by Fig. 11 (b) in [15]. We plan to address these open issues in a follow-up study.

Acknowledgments

We are grateful to the anonymous referee for valuable suggestions and comments. D.-H. Kim acknowledges financial support from the National Research Foundation of Korea (NRF) via Basic Research Grant NRF-2013R1A1A2008901. S. Trippe acknowledges financial support from the National Research Foundation of Korea (NRF) via Basic Research Grant NRF-2015R1D1A1A01056807. Correspondence should be addressed to S. T.

Appendix A: Non-polarized anisotropic incident radiation

In Subsection II A we prescribe an anisotropic incident monochromatic radiation field on a charge via the two waves,

$$\mathbf{E}_{\text{I(in)}} = E_{\text{I}} \{ \mathbf{e}_y \exp [i (Kx - \Omega t + \varphi_{\text{I}}(t))] + \mathbf{e}_z \exp [i (Ky - \Omega t + \vartheta_{\text{I}}(t))] \}, \quad (\text{A1})$$

$$\mathbf{E}_{\text{II(in)}} = E_{\text{II}} \{ \mathbf{e}_x \exp [i (Ky - \Omega t + \varphi_{\text{II}}(t))] + \mathbf{e}_z \exp [i (Kx - \Omega t + \vartheta_{\text{II}}(t))] \}, \quad (\text{A2})$$

where E_{I} and E_{II} ($E_{\text{I}} \neq E_{\text{II}}$) are the amplitudes, and Ω and K are the angular temporal frequency and angular spatial frequency with $\Omega = cK$, and $\varphi_{\text{I}}(t)$, $\vartheta_{\text{I}}(t)$, $\varphi_{\text{II}}(t)$ and $\vartheta_{\text{II}}(t)$ are the phase modulation functions, which are assumed to vary on a time scale much slower than the period of the waves, i.e. $|\dot{\varphi}_{\text{I}}|$, $|\dot{\vartheta}_{\text{I}}|$, $|\dot{\varphi}_{\text{II}}|$, $|\dot{\vartheta}_{\text{II}}| \ll \Omega$.

With this prescription, $\mathbf{E}_{\text{I(in)}}$ and $\mathbf{E}_{\text{II(in)}}$ are *unpolarized*. This is due to the relative phases $\varphi_{\text{I}}(t) - \vartheta_{\text{I}}(t)$ and $\varphi_{\text{II}}(t) - \vartheta_{\text{II}}(t)$ which fluctuate in time and will not let each wave remain in a single polarization state. This can be shown formally by computing the Stokes parameters out of the waves (A1) and (A2). By Eqs. (40) – (43) we calculate

$$I_{(\text{I})} = \left\langle |E_{\text{I } y(\text{in})}|^2 \right\rangle + \left\langle |E_{\text{I } z(\text{in})}|^2 \right\rangle, \quad (\text{A3})$$

$$Q_{(\text{I})} = \left\langle |E_{\text{I } y(\text{in})}|^2 \right\rangle - \left\langle |E_{\text{I } z(\text{in})}|^2 \right\rangle, \quad (\text{A4})$$

$$U_{(\text{I})} = \left\langle E_{\text{I } y(\text{in})} E_{\text{I } z(\text{in})}^* \right\rangle + \left\langle E_{\text{I } z(\text{in})} E_{\text{I } y(\text{in})}^* \right\rangle, \quad (\text{A5})$$

$$V_{(\text{I})} = i \left(\left\langle E_{\text{I } y(\text{in})} E_{\text{I } z(\text{in})}^* \right\rangle - \left\langle E_{\text{I } z(\text{in})} E_{\text{I } y(\text{in})}^* \right\rangle \right), \quad (\text{A6})$$

and

$$I_{(\text{II})} = \langle |E_{\text{II } x(\text{in})}|^2 \rangle + \langle |E_{\text{II } z(\text{in})}|^2 \rangle, \quad (\text{A7})$$

$$Q_{(\text{II})} = \langle |E_{\text{II } x(\text{in})}|^2 \rangle - \langle |E_{\text{II } z(\text{in})}|^2 \rangle, \quad (\text{A8})$$

$$U_{(\text{II})} = \langle E_{\text{II } x(\text{in})} E_{\text{II } z(\text{in})}^* \rangle + \langle E_{\text{II } x(\text{in})}^* E_{\text{II } z(\text{in})} \rangle, \quad (\text{A9})$$

$$V_{(\text{II})} = i \left(\langle E_{\text{II } x(\text{in})} E_{\text{II } z(\text{in})}^* \rangle - \langle E_{\text{II } x(\text{in})}^* E_{\text{II } z(\text{in})} \rangle \right). \quad (\text{A10})$$

From Eqs. (A1) and (A2) we easily find $\langle |E_{\text{I } y(\text{in})}|^2 \rangle = \langle |E_{\text{I } z(\text{in})}|^2 \rangle = E_{\text{I}}^2$ and $\langle |E_{\text{II } x(\text{in})}|^2 \rangle = \langle |E_{\text{II } z(\text{in})}|^2 \rangle = E_{\text{II}}^2$. However, for the cross-terms we find

$$\langle E_{\text{I } y(\text{in})} E_{\text{I } z(\text{in})}^* \rangle = \frac{E_{\text{I}}^2}{T} \int_0^T dt e^{i[\varphi_{\text{I}}(t) - \vartheta_{\text{I}}(t)]}, \quad (\text{A11})$$

$$\langle E_{\text{I } y(\text{in})}^* E_{\text{I } z(\text{in})} \rangle = \frac{E_{\text{I}}^2}{T} \int_0^T dt e^{-i[\varphi_{\text{I}}(t) - \vartheta_{\text{I}}(t)]}, \quad (\text{A12})$$

and

$$\langle E_{\text{II } x(\text{in})} E_{\text{II } z(\text{in})}^* \rangle = \frac{E_{\text{II}}^2}{T} \int_0^T dt e^{i[\varphi_{\text{II}}(t) - \vartheta_{\text{II}}(t)]}, \quad (\text{A13})$$

$$\langle E_{\text{II } x(\text{in})}^* E_{\text{II } z(\text{in})} \rangle = \frac{E_{\text{II}}^2}{T} \int_0^T dt e^{-i[\varphi_{\text{II}}(t) - \vartheta_{\text{II}}(t)]}. \quad (\text{A14})$$

For a sufficiently long time T , the phases $\pm[\varphi_{\text{I}}(t) - \vartheta_{\text{I}}(t)]$ and $\pm[\varphi_{\text{II}}(t) - \vartheta_{\text{II}}(t)]$ will fluctuate randomly and thus their trigonometric evaluations will be uniformly distributed over $[-1, 1]$ for $t \in [0, T]$. This will lead the integrals $\int_0^T dt e^{\pm i[\varphi_{\text{I}}(t) - \vartheta_{\text{I}}(t)]}$ and $\int_0^T dt e^{\pm i[\varphi_{\text{II}}(t) - \vartheta_{\text{II}}(t)]}$ to be finite and hence $\int_0^T dt e^{\pm i[\varphi_{\text{I}}(t) - \vartheta_{\text{I}}(t)]}/T$ and $\int_0^T dt e^{\pm i[\varphi_{\text{II}}(t) - \vartheta_{\text{II}}(t)]}/T$ to be vanishingly small. Therefore, we finally have

$$\begin{bmatrix} I_{(\text{I,II})} \\ Q_{(\text{I,II})} \\ U_{(\text{I,II})} \\ V_{(\text{I,II})} \end{bmatrix} = 2E_{\text{I,II}}^2 \begin{bmatrix} 1 \\ 0 \\ 0 \\ 0 \end{bmatrix}, \quad (\text{A15})$$

which was to be proved.

Appendix B: Solving the geodesic equation of motion for a charge in perturbed spacetime

In Section II A 1 the geodesic equation of motion for a charge in the spacetime $g_{\mu\nu} = \eta_{\mu\nu} + h_{\mu\nu}$ in linearized gravity reads

$$\ddot{X}^i + \eta^{ik} h_{jk,t} \dot{X}^j + \frac{1}{2} \eta^{il} (h_{jl,k} + h_{kl,j} - h_{jk,l}) \dot{X}^j \dot{X}^k = \frac{q}{m} (\eta^{ik} - h^{ik}) E_k, \quad (\text{B1})$$

where the GWs h_{ij} are given by

$$h_{ij}^+ = h (e_i^1 \otimes e_j^1 - e_i^2 \otimes e_j^2) \exp \left[i\omega \left(\frac{z}{c} - t \right) \right], \quad (\text{B2})$$

$$h_{ij}^\times = h (e_i^1 \otimes e_j^2 + e_i^2 \otimes e_j^1) \exp \left[i\omega \left(\frac{z}{c} - t \right) \right], \quad (\text{B3})$$

with h representing the strain amplitude, ω the frequency and $+/\times$ the two polarization states prescribed by the tensors $e_i^1 \otimes e_j^1 - e_i^2 \otimes e_j^2$ and $e_i^1 \otimes e_j^2 + e_i^2 \otimes e_j^1$, and on the right-hand side the EM field is given by

$$E_i = e_i^2 E_{\text{I}} \exp \left[i \left(\Omega \left(\frac{z}{c} - t \right) + \varphi_{\text{I}}(t) \right) \right] + e_i^1 E_{\text{II}} \exp \left[i \left(\Omega \left(\frac{z}{c} - t \right) + \varphi_{\text{II}}(t) \right) \right], \quad (\text{B4})$$

which describes the outgoing field reflected by the charge.

The geodesic equation (B1) can be solved via perturbation. First, the unperturbed part of a solution for $\dot{X}^i = (\dot{x}, \dot{y}, \dot{z})$, namely $\dot{X}_{[0]}^i = (\dot{x}_{[0]}, \dot{y}_{[0]}, \dot{z}_{[0]})$ is obtained as follows. Plugging $\dot{X}^i = \dot{X}_{[0]}^i$ into Eq. (B1), and keeping only the unperturbed terms, we have

$$\dot{X}_{[0]}^i = \frac{q}{m} \eta^{ik} E_k. \quad (\text{B5})$$

Inserting Eq. (B4) into Eq. (B5), and integrating this over t ,

$$\begin{aligned} \dot{X}_{[0]}^i &= v_o^i + \frac{q}{m} \eta^{ik} \int_0^t dt' E_k \\ &= v_o^i + \frac{q E_{oi}}{m} \int_0^t dt' \exp \left[i \left(\Omega \left(\frac{z}{c} - t' \right) + \varphi_i(t') \right) \right], \end{aligned} \quad (\text{B6})$$

where $E_{oi} = (E_{\text{II}}, E_{\text{I}}, 0)$ and $\varphi_i(t) = (\varphi_{\text{II}}(t), \varphi_{\text{I}}(t), 0)$. Now, we take the time-dependent part from the integral in Eq. (B6) and define

$$\mathcal{I}(t) \equiv \int_0^t dt' e^{-i[\Omega t' - \varphi(t')]}, \quad (\text{B7})$$

where $\varphi(t)$ refers to either $\varphi_{\text{I}}(t)$ or $\varphi_{\text{II}}(t)$. Using integration by parts repeatedly, we arrive at

$$\begin{aligned} \mathcal{I}(t) &= i \frac{e^{-i[\Omega t - \varphi(t)]}}{\Omega} \left\{ 1 + \frac{\dot{\varphi}(t)}{\Omega} + \left[\left(\frac{\dot{\varphi}(t)}{\Omega} \right)^2 - i \frac{\ddot{\varphi}(t)}{\Omega^2} \right] + \left[\left(\frac{\dot{\varphi}(t)}{\Omega} \right)^3 - 3i \frac{\dot{\varphi}(t)}{\Omega} \frac{\ddot{\varphi}(t)}{\Omega^2} - \frac{\ddot{\varphi}(t)}{\Omega^3} \right] + \dots \right\} \\ &= i \frac{e^{-i[\Omega t - \varphi(t)]}}{\Omega} + \mathcal{O}_{[0]}(\dot{\varphi}/\Omega, \ddot{\varphi}/\Omega^2, \dot{\varphi}\ddot{\varphi}/\Omega^3, \ddot{\varphi}/\Omega^3, \dots) \end{aligned} \quad (\text{B8})$$

where $\dot{\varphi}/\Omega \sim \varepsilon$, $\ddot{\varphi}/\Omega^2 \sim \varepsilon^2$, $\dot{\varphi}\ddot{\varphi}/\Omega^3 \sim \ddot{\varphi}/\Omega^3 \sim \varepsilon^3$, etc. with $\varepsilon \ll 1$, from the assumption that $\varphi(t)$ varies on a time scale much slower than the period of the wave, i.e. $|\dot{\varphi}| \ll \Omega$, $|\ddot{\varphi}| \ll \Omega^2$, $|\dot{\varphi}\ddot{\varphi}| \ll \Omega^3$, etc. This leads to

$$\dot{X}_{[0]}^i = v_o^i + i \frac{q E_{oi}}{m \Omega} \exp \left[i \left(\Omega \left(\frac{z}{c} - t \right) + \varphi_i(t) \right) \right] + \mathcal{O}_{[0]}(\dot{\varphi}_i/\Omega, \ddot{\varphi}_i/\Omega^2, \dot{\varphi}_i \ddot{\varphi}_i/\Omega^3, \ddot{\varphi}_i/\Omega^3, \dots). \quad (\text{B9})$$

A first-order perturbation of \dot{X}^i , namely $\dot{X}_{[h]}^i$ is obtained by recycling the unperturbed part, i.e. Eq. (B9) into Eq. (B1). Plugging $\dot{X}^i = \dot{X}_{[0]}^i + \dot{X}_{[h]}^i$ into Eq. (B1), and keeping only first-order terms in h ,

$$\dot{X}_{[h]}^i = -\frac{q}{m} h^{ik} E_k - \eta^{ik} h_{jk,t} \dot{X}_{[0]}^j - \frac{1}{2} \eta^{il} (h_{jl,k} + h_{kl,j} - h_{jk,l}) \dot{X}_{[0]}^j \dot{X}_{[0]}^k. \quad (\text{B10})$$

Integrating this over t ,

$$\dot{X}_{[h]}^i = -\frac{q}{m} \int_0^t dt' h^{ik} E_k - \eta^{ik} \int_0^t dt' h_{jk,t'} \dot{X}_{[0]}^j - \frac{1}{2} \eta^{il} \int_0^t dt' (h_{jl,k} + h_{kl,j} - h_{jk,l}) \dot{X}_{[0]}^j \dot{X}_{[0]}^k, \quad (\text{B11})$$

where the integrands are specified by Eqs. (B2), (B3), (B4) and (B9). Here each integral has the same form as Eq. (B7) and hence can be approximated in the same manner as in Eq. (B8), thereby generating the error $\mathcal{O}_{[h]}(\dot{\varphi}/\Omega, \ddot{\varphi}/\Omega^2, \dot{\varphi}\ddot{\varphi}/\Omega^3, \ddot{\varphi}/\Omega^3, \dots) \sim h \times \mathcal{O}_{[0]}(\dot{\varphi}/\Omega, \ddot{\varphi}/\Omega^2, \dot{\varphi}\ddot{\varphi}/\Omega^3, \ddot{\varphi}/\Omega^3, \dots)$. Combining the result from Eq. (B11) with Eq. (B9), we obtain the full first-order perturbation solution, i.e. $\dot{X}^i = \dot{X}_{[0]}^i + \dot{X}_{[h]}^i$, which has the total error $\mathcal{O}_{[0]}(\dot{\varphi}/\Omega, \ddot{\varphi}/\Omega^2, \dot{\varphi}\ddot{\varphi}/\Omega^3, \ddot{\varphi}/\Omega^3, \dots) + \mathcal{O}_{[h]}(\dot{\varphi}/\Omega, \ddot{\varphi}/\Omega^2, \dot{\varphi}\ddot{\varphi}/\Omega^3, \ddot{\varphi}/\Omega^3, \dots)$, as presented in Eqs. (14) – (19).

The full first-order perturbation solution for \ddot{X}^i , i.e. $\ddot{X}^i = \ddot{X}_{[0]}^i + \ddot{X}_{[h]}^i$ can be obtained by combining Eqs. (B5) and (B10). The unperturbed part $\ddot{X}_{[0]}^i$ is trivially obtained from the right-hand side of (B5), which is equivalent to E_i (B4) apart from the factor; thereby not generating $\mathcal{O}_{[0]}$. However, the perturbed part $\ddot{X}_{[h]}^i$ is obtained by recycling the unperturbed part $\dot{X}_{[0]}^i$ (B9) into (B10); thereby generating the error $\mathcal{O}_{[h]} \sim h \times \mathcal{O}_{[0]}$. Hence the total error from $\ddot{X}^i = \ddot{X}_{[0]}^i + \ddot{X}_{[h]}^i$ is $\mathcal{O}_{[h]}$ only. The rescattered EM radiation is obtained by

$$E_{(\text{scat})}^i = \frac{q \ddot{X}^i}{r} = \frac{q}{r} \left(\ddot{X}_{[0]}^i + \ddot{X}_{[h]}^i \right), \quad (\text{B12})$$

due to Eqs. (23), (24) and (25), and therefore it has the error $\mathcal{O}_{[h]}$ only, as shown by Eqs. (26) - (31).

-
- [1] Ade, P. A. R. & PLANCK Collaboration 2014, A&A, 571, A16
 - [2] Ade, P. A. R. & BICEP2 Collaboration 2014, Phys. Rev. Lett., 112, 241101
 - [3] Ade, P. A. R. & POLARBEAR Collaboration 2014, Phys. Rev. Lett., 113, 021301
 - [4] Ade, P. A. R. & POLARBEAR Collaboration 2015, Publ. Korean Astron. Soc., 30, 625
 - [5] Bahcall, N. A., Ostriker, J. P., Perlmutter, S., & Steinhardt, P. J. 1999, Science, 284, 1481
 - [6] Barkats, D. & BICEP1 Collaboration 2014, ApJ, 783, 67
 - [7] The Cardiff Gravitational Physics Group tutorial: Observing relic gravitational waves, <http://www.astro.cardiff.ac.uk/research/gravity/tutorial>
 - [8] Chandrasekhar, S. 1960, *Radiative Transfer*, 1st edn. (Dover Publications Inc., New York)
 - [9] Chiang, C.-T. & Komatsu, E. 2011, *CMB Polarization from Gravitational Waves – Reversed Power of Tensor E-modes and B-modes for $l < 50$ in Reionized Universe*, poster at DEUS conference, Copenhagen, http://wwwmpa.mpa-garching.mpg.de/~ctchiang/docs/posters/cmb_polar_reion_ctchiang_2011.pdf
 - [10] Dicke, R. H., Peebles, P. J. E., Roll, P. G., & Wilkinson, D. T. 1965, ApJ, 142, 414
 - [11] Flauger, R., Hill, J. C., & Spergel, D. N. 2014, J. Cosmology Astropart. Phys., 8, 39
 - [12] Goldstein, H. 1980, *Classical Mechanics*, 2nd edn. (Addison-Wesley Publishing Company, Inc., USA, 1980)
 - [13] Halonen, R. J., Mackay, F. E., & Jones, C. E. 2013, ApJS, 204, 11
 - [14] Hanson, D. & SPTpol Collaboration 2013, Phys. Rev. Lett., 111, 141301
 - [15] Hu, W. & White, M. 1997, New Astron. 2, 323
 - [16] Hu, W. & White, M. 1997, Phys. Rev. D, 56, 596
 - [17] Kamionkowski, M., Kosowsky, A., & Stebbins, A. 1997, Phys. Rev. D, 55, 7368
 - [18] Kim, J. 2011, A&A, 531, A32
 - [19] Kovac, J. M. et al. 2002, Nature, 420, 772
 - [20] Martin, J., Ringeval, C., & Vennin, V. 2014, Phys. Dark Universe, 5, 75
 - [21] Naess, S. & ACT Collaboration 2014, J. Cosmolog. Astropart. Phys., 10, 7
 - [22] Newman, E. & R. Penrose, R. 1966, J. Math. Phys., 7, 863
 - [23] Pai, A., Dhurandhar, S., & Bose, S. 2001, Phys. Rev. D, 64, 042004
 - [24] D. Papadopoulos, D. 2002, A&A, 396, 1045
 - [25] Penzias, A. A., & Wilson, R. W. 1965, ApJ, 142, 419
 - [26] Polnarov, A. G. 1985, Sov. Astron., 29, 607
 - [27] Ruffini, R. & Sasaki, M. 1981, Prog. Theor. Phys., 66, 1627
 - [28] Trippe, S. 2014, J. Korean Astron. Soc., 47, 15
 - [29] Zaldarriaga, M. & Seljak, U. 1997, Phys. Rev. D, 55, 1830